Chapter 4
Control of Liquids by Surface Energies

Martin Brinkmann, Krishnacharya Khare, and Ralf Seemann

Max-Planck Institute for Dynamics and Self-Organization,
Göttingen (Germany)
martin.brinkmann@ds.mpg.de
krishnacharya.khare@ds.mpg.de
ralf.seemann@ds.mpg.de

1. Introduction

Our every day experience of handling liquids is strongly linked to the presence of gravity. In a zero gravity environment, as realized during parabola flights or in space crafts, it is almost impossible to pour water from a bottle into a glass. A close look at a glass of water already reveals the influence of interfacial energies: the curvature of the water meniscus bends up close to its rim due to the high wettability of clean glass surfaces by water. When compartmentalized into structures smaller than a characteristic length being typically on the order of 1 mm gravity becomes irrelevant and interfacial energies dominate both the statics and dynamics of a liquid down to a length scale of about 10 nm [1].

The strong impact of interfacial energies on the morphology of sub-millimeter-sized wetting droplets can be utilized to control the position and the shape of tiny amounts of liquid on specifically designed substrates. Figure 1 shows a comparison of droplet shapes on a plane substrate decorated with a pattern of wettable stripes (left) and a structure of rectangular grooves on a chemically homogeneous substrate (right). Wettability patterns on the substrate or surface topographies may act as “anchoring points” for the contact line of the wetting liquid.

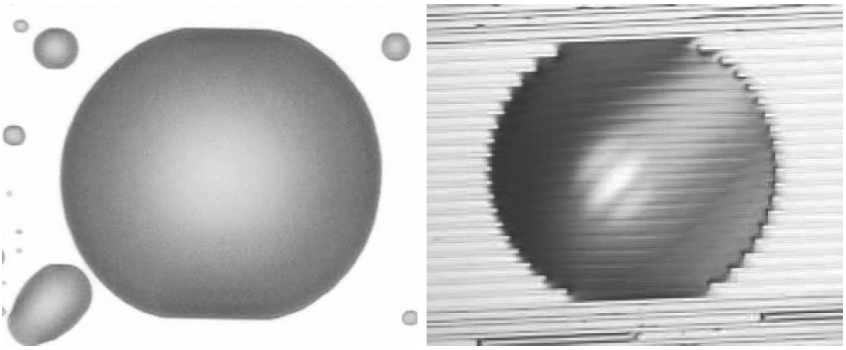

Fig. 1. Hexaethylene glycol droplet on a plane substrate bearing horizonal wettable stripes (left) with a periodicity of 400 nm in comparison to a polymer droplet on a topographically structured substrates with rectangular grooves (right). Pinning of the three phase contact line is clearly visible from the non-spherical shape of the droplets perimeter (left image taken from Herminghaus et al. [2] with kind permission of Springer Science and Business Media)

Highly wettable stripes on plane substrates can provide the means to guide a liquid on a surface [3–6]. Changes in the adhesion energy of the liquid can be utilized to fill linear surface topographies such as rectangular grooves [7, 8]. Therefore, chemical patterns and topographic structures such as grooves represent potential building blocks of open microfluidic systems [9], alternative to closed systems fabricated in a solid matrix.

For fundamental physical understanding, but as well for potential use in printing techniques [4, 10, 11], soldering [12–14], biotechnological applications [15] or open microfluidics [3, 8, 9, 16, 17], wetting of chemically or topographically structured surfaces by nonvolatile liquids has become a topic of intense research in recent years. The proper functioning of wettability-based systems requires a full understanding of the liquid behavior for a variety of different substrate designs. Here, in particular, the pioneering work in the group of Lipowsky on the theoretical framework of morphological wetting on chemically structured substrates has to be mentioned [1, 3, 5, 18–21]. Experimental and theoretical studies of basic liquid morphologies have been performed for various wettability patterns and surface topographies. This includes circular domains [18–20], stripes [3, 5], rings of different wettability [21, 22] as well as topographic steps [7] and channels of triangular [23, 93] or rectangular cross section [8, 23].

Wettability patterns and substrate topographies imprinted to the surface are typically static. Here, the morphology can be controlled by liquid volume. Potential applications in open microfluidics require an active control of liquid morphologies of given volume. This can be achieved with techniques

to switch the wettability by external stimuli. Here, the electrowetting effect provides a versatile tool to reversibly switch contact angles of conductive wetting liquids [9, 24].

In the following Sect. 2, we will give an outline of the fundamental wetting phenomena involved in the description of liquid morphologies and their transitions on chemically and topographically structured substrates. Section 3 is devoted to plane substrates decorated with basic patterns of differently wettable domains. A short overview of available experimental preparation techniques is included in this section. Results for wetting morphologies on topographically structured substrates are summarized in the subsequent Sect. 4, which, again, includes a short introduction to experimental techniques. We present an application of a particular morphological transition that can be utilized to control the imbibition of liquid into topographic structures.

2. Capillary Model

Small insects like the water strider *Gerris remigis* have the astonishing ability to move on a water surface [25]. The weight of the water strider is balanced by interfacial forces of the water–air interface. An increase of the area of the liquid–vapor interface requires work against interfacial tension. The water strider could walk on any liquid provided the strider's weight is small enough. If the deformations of the water interface around the strider's feet are small, the accompanying increase of interfacial free energy scales with the square of the indentation depth in contrast to the gravitational energy that decreases linearly, leading to a stable mechanical equilibrium.

Interfacial free energies can be obtained, in principle, as the excess of total free energy of the system over the free energy of the bulk phases [26]. This surface excess of the free energy can be easily explained from the microscopic interactions between liquid molecules at or close to the interface. Creating new interfacial area between two fluid phases requires to break bonds between neighboring molecules and is therefore related to an energy increase. A negative sign of the interfacial energy would contradict the mechanical stability of the two fluid phases in coexistence.

Details of the molecular interactions, however, are not relevant on macroscopic length scales where the interfacial energies and the spatial configuration of the liquid–vapor interface contains all necessary information about the system. These details are essential only in microscopic models of the liquid interface, for instance, in a description of the density profile

between the liquid and an adjacent bulk phase. For all practical purposes, the intrinsic width of the interface and the interfacial roughness caused by thermal fluctuations are many orders of magnitude smaller than the size of the droplets [27]. Hence, in the framework of the following discussion, we regard all interfaces as mathematical surfaces, i.e., ideal interfaces of zero width. As shown experimentally, this assumption stays valid even for mesoscopic liquid droplets with lateral dimensions below 100 nm [6, 28, 29].

2.1. Equilibrium Conditions

For nonvolatile and incompressible liquids, the mechanically stable droplet shapes are determined by a local minimum of interfacial and gravitational energy. Contributions of gravitational energy are negligibly small if the droplet size is well below the capillary length

$$\ell_c = \sqrt{\frac{\gamma_{lv}}{g\,|\Delta\rho|}}\,, \tag{1}$$

which is determined from a balance of gravitational and interfacial energies. In expression (1), γ_{lv} is the interfacial tension of the liquid–vapor interface, $\Delta\rho = \rho_l - \rho_v$ the density difference between the liquid l and vapor v, and g the normal acceleration. Typically, ℓ_c is on the order of 1 mm. Because of the large interfacial tension between water and air, the related capillary length has a comparably large value $\ell_c \approx 2.7$ mm. For special systems, the capillary length ℓ_c can assume values on the order of centimeters, or may become even larger if the ambient phase is an immiscible liquid with a density close to the density of the wetting liquid. In this way, the effect of gravity or, to be precise, of buoyancy on the wetting liquid can be drastically reduced in capillary experiments.

The liquid–vapor interface of a wetting morphology with dimensions well below ℓ_c is a surface of constant mean curvature in mechanical equilibrium. The mean curvature H and the interfacial tension γ_{lv} of the liquid–vapor interface are related to the difference $\Delta P = P_l - P_v$ between the pressure P in the liquid l and the ambient vapor phase v by the Laplace equation

$$\Delta P = 2H\gamma_{lv}\,. \tag{2}$$

The local mean curvature $H = (C_1 + C_2)/2$ is the arithmetic mean of the principal curvatures C_1 and C_2 in the respective point of the surface [30], as illustrated in the sketch Fig. 2a. The liquid–vapor interface of a spherical droplet found on plane substrates has a normal curvature $C = 1/R$ irrespective of the direction and the point on the surface. Hence, a spherical surface is a surface of constant mean curvature with $H = 1/R$, where R is the radius of the sphere.

The equation of Laplace (2) is still valid for liquid–vapor interfaces with a vertical extension on the order or larger than ℓ_c. Here, the pressure difference in the respective point of the liquid–vapor interface includes a contribution of the hydrostatic pressure in the fluid phases. Corrections to the Laplace pressure have to be introduced for liquid structures of size smaller than a mesoscopic length ℓ_m. This disjoining pressure is mostly due to long ranged van der Waals or electrostatic forces, which become relevant for liquid structures on the substrate with a vertical extension smaller than roughly ℓ_m 10 nm [6]. For these two cases, i.e., in the range of droplet dimensions above ℓ_c and droplet dimensions below ℓ_m, the liquid–vapor interface cannot be approximated by a surface of constant mean curvature.

In mechanical equilibrium, the liquid–vapor interface of a wetting droplet meets the surface of the substrate at a constant angle θ, which is solely

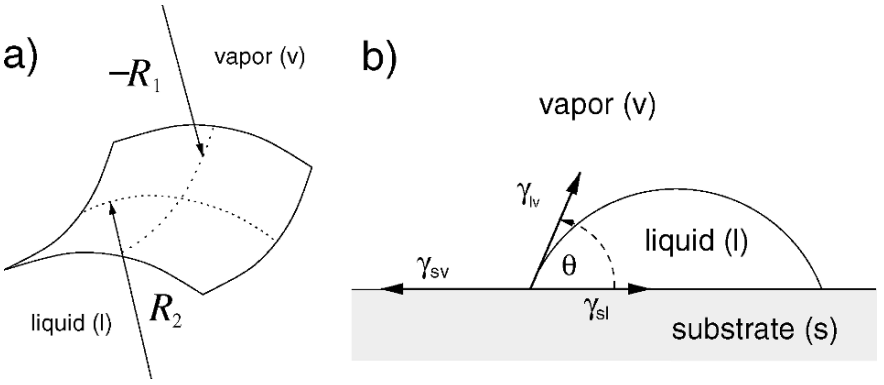

Fig. 2. (**a**) The mean curvature H of the liquid–vapor interface is the sum divided by two of the principal curvatures $C_1 = 1/R_1$ and $C_2 = 1/R_2$. Note, that the sign of the normal mean curvatures depends on the orientation of the surface. By definition, the curvature of a sphere is positive. (**b**) Sketch of the balance of interfacial forces at the three phase contact line

determined by interfacial tensions $\gamma_{lv}, \gamma_{sl}, \gamma_{sv}$ of the respective interfaces, cf. Fig. 2b. The equation of Young-Dupré

$$\cos\theta = \frac{\gamma_{sv} - \gamma_{ls}}{\gamma_{lv}}, \tag{3}$$

expresses the mechanical equilibrium of the three phase contact line between the substrate, the vapor, and the wetting liquid. The equilibrium contact angle θ, or the "material" contact angle, is a direct measure of the substrate wettability. According to the Greek terms for "water loving" and "water hating" contact angles $\theta < 90°$ have been termed hydrophilic while contact angles with $\theta > 90°$ are referred to as hydrophobic, respectively. In the sequel, these terms are not restricted to water and will be used for any wetting liquid.

2.2. Contact Line Pinning

The equation of Young-Dupré, (3), may become ill-defined on plane surfaces with a discontinuous dependence of the surface tensions γ_{ls} and γ_{vs} on the position. The contact angle θ in points of the contact line coinciding with such a discontinuity can attain any value between the smaller value θ_- on the more hydrophilic side and the larger value θ_+ on the more hydrophobic side of the discontinuity, cf. Fig. 3a. As a consequence, the contact line is immobilized and its position is fixed to the line of discontinuity as long as the contact angle falls into the range between

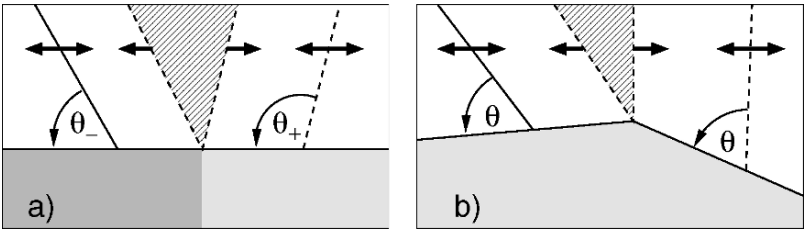

Fig. 3. Sketch of a wetting front moving over a wettability step or a kink in the substrate topography. (**a**) The three phase contact line becomes pinned to a boundary between two differently wettable domains with contact angles θ_- and θ_+ as long as the position of the liquid–vapor interface remains in the hatched sector. (**b**) Pinning of the contact line to a convex edge on a homogeneous substrate

θ_- and θ_+. Hence, the contact angle is not defined by the local wettability of the substrate but depends on the global shape of the liquid–vapor interface in equilibrium.

The sketch in Fig. 3b illustrates the pinning of a moving contact line at a convex edge of a topography on a substrate with homogeneous wettability. Any configuration of the liquid–vapor interface that forms a contact angle larger than the equilibrium contact angle θ according to (3) with respect to the left side of the kink and a contact angle smaller than the contact angle θ with respect to the right side of the kink can be in equilibrium. Because of its enlarged free range of contact angles, an acute convex edge of the substrate pins the contact line more effectively than less acute edges. Concave corners, contrary to convex edges, cannot immobilize the contact line. Configurations of the liquid–vapor interface with a contact line that is fully or partially aligned with a concave corner of the topography are unstable.

As we will see in the following, constraining the contact line to certain positions on chemically or topographically structured substrates allows the liquid to form a large variety of equilibrium shapes.

2.3. Computation of Droplet Shapes

Surfaces decorated with wettability patterns or substrate topographies lead to complex equilibrium morphologies of the wetting liquid due to the pinning mechanisms mentioned above. According to the Laplace equation (2), the liquid–vapor interface of small droplets substrates will always be a surface of constant mean curvature even on heterogeneous substrates. The size of the droplets shall be small compared to the capillary length ℓ_c but still large compared to the mesoscopic length ℓ_m. The vast majority of these equilibrium shapes cannot be parameterized explicitly, even for substrates with regular wettability patterns or surface topographies. Hence, the main features of the liquid–vapor interface may be partially captured through a substitution of the real configuration by known surfaces of constant mean curvature if the dimensions of these liquid structures fall into this range of length scales. Possible shape “primitives” are segments of cylinders [7, 8], parts of a sphere [18], or even suitable pieces of a Delaunay surface [20, 21]. The family of Delaunay surfaces comprises all surfaces of revolution with constant mean curvature being periodic along the axis of symmetry. The surface of a sphere and the catenoid are obtained as limiting shapes while the cylinder is a special Delaunay surface [21].

Generically, the condition of Young-Dupré will not be matched in all points of the contact line. The shape of a primitive is fixed by a low dimensional set of parameters like, for instance, the radius and the contact angle of a spherical cap. Within such an approximation, the interfacial energy of the model droplet is a function of these parameters and can be analytically minimized while respecting the constraint of a constant liquid volume. This method has been successfully applied to several problems, calculating the equilibrium shapes of liquid filaments on wettable stripes [5], topographic steps [7], and rectangular grooves [8]. In some rare cases one may obtain exact analytic solution in this way, i.e., surfaces of constant mean curvature whose boundaries are consistent with the equation of Young-Dupré (3) or the condition of a pinned contact line [20].

Alternative to approximations by shape primitives, the liquid–vapor interface may be represented by a mesh of small triangles spanning between neighboring nodes. A large number of theoretical investigations in the field of wetting on structured surfaces have been performed using this numerical model. The interfacial energy of such a discrete, polyhedral surface is a function of $3N$ coordinates where N is the number of nodes which make up the mesh. Global constraints like a constant droplet volume or local constraints that have to be enforced, for instance, on those nodes gliding on the substrate walls are respected during minimization. Flipping of edges changes the topology of the mesh which is necessary to adapt to changes in the configuration during morphological transitions. New edges can be introduced to the mesh while short edges are constantly removed. In this way, the distribution of edge lengths on the polyhedral surfaces is kept in a certain desired range. Numerical minimizations using such a dynamically triangulated model of the liquid–vapor interface can be performed with the public domains software "surface evolver," developed by K. Brakke [31]. This program offers a whole script language to define the substrate geometry and required energies, methods for mesh manipulation, and a number of minimization schemes.

3. Plane Substrates with Wettability Patterns

On plane and chemically homogeneous substrates, small droplets attain the shape of spherical caps, as discussed in Sect. 2. Qualitatively different droplet shapes emerge on surfaces decorated with patterns of differently wettable domains. Driven by the minimization of interfacial energy, the liquid tries to maximize the contact area with the highly wettable surface domains and to avoid the poorly wettable parts of the substrate. In a certain

range of liquid volumes and wettabilities, the wetting liquid follows the geometry of the wettable structures and is restricted by the boundaries of the highly wettable domains. Here, contact line pinning is the central feature that governs the morphology of liquid on chemically structured substrates.

Before we discuss liquid morphologies on several fundamental wettability patterns, we briefly summarize in the following Sect. 3.1 common experimental techniques by which wettability patterns and liquid morphologies can be created and analyzed. Contact line pinning and equilibrium morphologies of liquid on chemically structured surfaces are illustrated in Sect. 3.2 for the particular geometry of an array of highly wettable circular domains embedded in a poorly wettable matrix. We will discuss the equilibrium liquid morphologies depending on control parameter such as the contact angles θ_- and θ_+ on the highly and poorly wettable domains, respectively, and the liquid volume V. Furthermore, we extend the complexity of the chemical patterns to lines and rings, and consider morphological wetting transition on these substrates in Sect. 3.3.

3.1. Experimental

The smoothest surfaces with chemical contrast can be found in semiconductor industry. If two crystalline materials are combined or troughs of a crystalline material are "filled" by epitaxial growth, these surfaces can be polished to an almost atomically smooth surface. Unfortunately this technique is very expensive and the range of available materials, i.e., wettabilities and pattern shapes is very limited.

Hence, for scientific experiments, the wettability of surfaces is typically tailored by grafting self assembly monolayers onto surfaces. This preparation technique allows to vary the contact angle within a fairly large range up to about 115° for water. Self assembly monolayers of certain molecules form a closed monomolecular coating, which might be covalently bonded to the respective surface [32]. By the nature of a monolayer, its thickness is given by the extension of the molecules, which is typically on the order of one nanometer. The head groups of the molecules, which bind to glass or silicon oxide surfaces are often mono- and trichlorosilanes. In case of gold surfaces, thiols are used. Generally, the trichlorosilanes layer are more stable than monochlorosilanes as expected by the larger number of possible binding sites, but have the tendency to form multilayers. For the typically hydrophobic wetting properties, the tail group of the molecules usually consists of alkyl chains, which might be perfluorinated.

Basically, there are two possibilities to fabricate chemically patterned substrates. The first strategy is to start with a homogeneous SAM-layer and remove or oxidize the molecules in order to achieve the desired wettability pattern, e.g., by exposure to UV/ozone or oxygen plasma [33–35], through dewetting patterns [36], or by electrochemistry using patterned electrodes [37]. Very fine wetting structures can be achieved by locally oxidizing the substrate or removing the SAM-layer by electrochemistry applying a voltage between the substrate and the tip a scanning force microscope (SFM) [38–42].

The second strategy is to directly graft a SAM-layer only to specific areas of a substrate. One may start with a prepatterned substrate where the SAM-layer binds selectively to parts of the surface with a certain chemical composition. As prepatterns, often thin gold layers are vapor deposited through masks like transmission electron microscopy (TEM) grids [3, 43], or created by colloidal monolayer [44–46], breath figures [47], and dewetting or microphase separation patterns [48]. These masks can furthermore be used to create hydrophilic patterns by vapor deposition of hygroscopic salts like $CaCl_2$ or MgF_2 [3, 43].

Alternatively, SAM-layers can be patterned directly, e.g., by domain formation in Langmuir-Blodget monolayers transferred to solid substrates [49] or unstable monolayers produced by such a monolayer transfer [50]. Unfortunately, the spectrum of possible wetting patterns is very limited. The only patterns, for instance, which can be created by the latter technique, are parallel stripes. A much more flexible method, but technically demanding, is the dip pen lithography where lines are written onto a substrate by an SFM tip similar to a fountain pen [51–53]. A straight forward and easy to use method is the so-called microcontact printing [54–57]. Here, molecules that are able to form a SAM-layer are printed to a substrate by the raised parts of a poly(dimethyl siloxane) rubber (PDMS) stamp. To avoid multi-layer formation in microcontact printing preferably monochlorosilanes are used. This soft lithography technique works well for structure sizes down to about 100 nm.

The liquid morphologies are typically created by condensing liquid from the vapor phase onto the patterned surface [3, 43, 50, 59], dip coating the substrates [4, 10, 11], or dewetting liquid from a substrate [60, 61]. Often, organic fluids or water are used as wetting liquids. The liquids might be cooled or osmotically stabilized allowing for an extended observation time [3, 59]. Liquids that can be solidified without remarkable volume change allow for a long term stability of the formerly liquid morphologies and an exact three-dimensional analysis of its shape. Polymers like polystyrene can be solidified by temperature [8], UV-curable prepolymers can be

solidified by exposure to light [56, 62], and metal oxide morphologies can be created from an organic sol–gel solution [19, 63].

Optical microscopy techniques are the main investigation tool to characterize the emerging liquid morphologies. These optical techniques are limited in lateral resolution and their ability to analyze the structures in three-dimensions. A quantitative three-dimensional analysis of the wetting morphologies is possible up to a contact angle of about 25°, only. The surface of a solidified liquid droplet can be imaged by atomic force microscopy (AFM) or scanning electron microscopy (SEM), which overcome the limitations of the optical techniques regarding the lateral resolution and the maximal contact angle. Even liquid structures can be imaged by AFM in tapping mode™ [59] or environmental SEM [64].

3.2. Circular Surface Domains

It is instructive to start our consideration with a surface pattern of circular hydrophilic domains on a hydrophobic substrate matrix. This ensures that the equilibrium droplet shapes on the patterned substrate are still segments of a sphere which, in return, allows an analytical description of the system. Morphological transitions between different equilibrium configurations of liquid distributed to an array of hydrophilic discs were first addressed by Lenz and Lipowsky [18]. Bechinger et al. performed experiments for the inverse geometry of wetting layers on a hydrophobic matrix that is perforated by an array of circular hydrophobic domains [19]. The morphology of the liquid film and its instabilities were analyzed theoretically by Lenz et al. [20].

A sufficiently small amount of liquid placed onto a circular hydrophilic domain forms a spherical cap with a contact angle given by the material contact angle $\theta_- < 90°$. In this regime (I), the contact line of the small droplet has a circular shape and is completely located on the highly wettable domain, cf. Fig. 4. While adding more liquid, the droplet grows until it covers the entire domain. At this point, the contact line coincides with the circular domain boundary. This regime of pinned droplet configurations is referred to as regime (II). During a further increase of the droplet volume, the position of the contact line remains fixed to the boundary while the contact angle θ grows until it reaches the limiting value given by the contact angle θ_+ on the less wettable substrate matrix. Beyond this point, the contact line of the spherical droplet detaches from the boundary and slides onto the hydrophobic, respectively, less hydrophilic matrix, cf. regime (III) in Fig. 4.

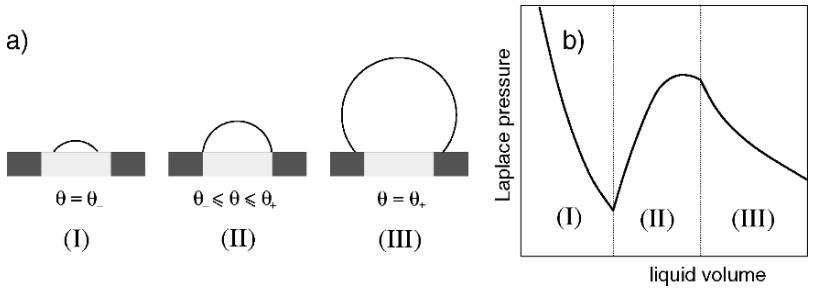

Fig. 4. Spherical droplet on a highly wettable domain of circular shape for different liquid volumes (**a**) and the corresponding Laplace pressure (**b**) according to Lenz and Lipowsky [18]. In regime (I) and (III), the Laplace pressure is a strictly monotonously decreasing function of the liquid volume. The Laplace pressure increases with growing volume in regime (II) if the contact angle θ is below $90°$

The Laplace pressure ΔP of a liquid droplet on a homogeneous and plane surface is a monotonously decreasing function of the liquid volume V. This applies to droplets in regime (I) and (III), as sketched in Fig. 4. The Laplace pressure of a pinned droplet in regime (II) with $\theta < 90°$, however, is a monotonously growing function of the droplet volume. The Laplace pressure of a droplet in regime (II) attains a local maximum either at the boundary between regime (II) and (III), i.e., at a contact angle $\theta = \theta_+$ for $\theta_+ \leq 90°$, or at a contact angle $\theta = 90°$ for $\theta_+ \geq 90°$.

3.2.1. Array of Hydrophilic Discs

An array of N droplets on N circular hydrophilic domains has been considered for a full wettability contrast $\theta_- = 0°$ and $\theta_+ = 180°$ by Lenz and Lipowsky [18]. For this particular choice of material contact angles, the droplets are always found in the pinned regime (II). It is assumed that the droplets can exchange liquid volume, e.g., via the vapor phase. A homogeneous configuration of equally sized droplets with a contact angle $\theta < 90°$ is found for small volumes, cf. Fig. 5. At a total volume $V^* = 2\pi Na^3/3$, the contact angle of the droplets reaches the critical value $90°$, as shown in Fig. 5. Beyond V^*, the homogeneous droplet configuration is unstable with respect to an exchange of liquid volume. Since the Laplace pressure is a monotonously decreasing function of V for $\theta > 90°$, any small perturbation in the distribution of volume is amplified and leads to a heterogeneous droplet configuration. In equilibrium and, hence, in the

globally stable configuration for $V > V^*$, the Laplace pressure has to be the same in all droplets. Because there are only two possible droplet shapes for a given Laplace pressure, a small droplet with $\theta < 90°$ and a large droplet with $\theta > 90°$, the final droplet configuration has to be bimodal. But since two or more large droplets with $\theta > 90°$ cannot be mechanically stable with respect to an exchange of volume, the only possible locally stable equilibrium configuration is one large droplet in coexistence with $N - 1$ small droplets.

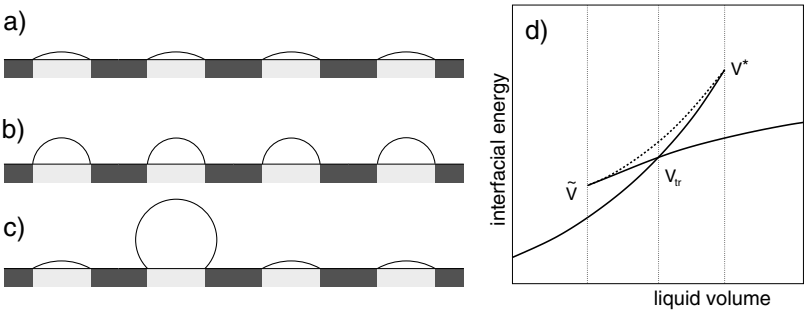

Fig. 5. Morphological transition between a homogeneous configuration of four small droplets (**a**) and (**b**), and a heterogeneous configuration (**c**) according to Lenz and Lipowsky [18]. The configuration in (**b**) with $\theta = 90°$ corresponds to the largest total volume V^* where the homogeneous configuration represents a local minimum of the interfacial energy. (**d**) Schematic hysteresis loop for the morphological transition between (**a**) and (**c**). The *solid line* on the lower left side of the diagram corresponds to the homogeneous configuration, the full line on the upper right side to the heterogeneous configuration. A branch of mechanically unstable solutions (*dashed line*) connects the branches of stable (or metastable) solutions. Note that the real hysteresis loop for $N = 4$ is extremely narrow and asymmetric

The transition between the homogeneous and heterogeneous droplet configurations is continuous for $N = 2$ [65]. In case of $N > 2$, however, the transition is hysteretic with respect to changes in the total volume V, i.e., the droplet configuration is not uniquely defined by V. An inverse transition from the heterogeneous to the homogeneous configuration occurs at a volume $\tilde{V} < V^*$ that depends on the total number of droplets N. The interfacial energy of the droplet configuration at its respective point of instability jumps to a smaller value during the shape transitions, cf. Fig. 5. Thus, there exists a liquid volume V^{tr} with $\tilde{V} < V^{\mathrm{tr}} < V^*$, where the interfacial free energies of both droplet configurations are identical. Many

features of this simple system are generic for transitions between different wetting morphologies, as we will demonstrate in the following.

3.2.2. Array of Hydrophobic Discs

The "inverse" geometry of a periodic array of circular hydrophobic surface domains on a hydrophilic substrate matrix has been investigated experimentally by Bechinger et al. [19] and later theoretically described by Lenz et al. [20]. Figure 6 shows a solidified wetting layer on a hexagonal lattice of circular hydrophobic domains after dewetting in comparison to numerical minimization of the interfacial energy. In their theoretical analysis, Lenz et al. assumed a perfectly wettable substrate and a separation distance between the circular domains, which is on the order of their diameter. The circular hydrophobic domains are arranged in a periodic lattice structure. It is useful to exploit the various symmetries of the system in numerical minimizations of the interfacial energy. Hence, one may consider only a unit cell of the surface pattern with appropriate periodic boundary conditions or even a smaller piece of the system by virtue of the discrete symmetries of the unit cell [20]. Possible instabilities of the liquid–vapor interface, which are accompanied by a redistribution of liquid on length scales larger than the size of a unit cell, are effectively suppressed.

If the thickness of the wetting layer is large compared to the distance between the holes, a plane liquid–vapor interface represents the configuration of the smallest interfacial energy. For small layer thicknesses, it is

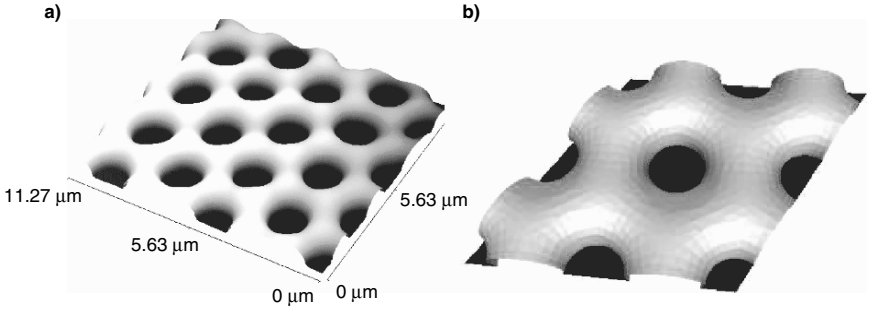

Fig. 6. (**a**) AFM micrograph showing a perforated wetting layer of gel-like hydrated WO_3 on a hexagonal array of hydrophobic circular discs (reprinted from Bechinger et al. [19], with permission from Elsevier). (**b**) Configuration of the liquid–vapor interface obtained by numerical minimization of the interfacial energy in the same geometry

energetically more favorable for the liquid to dewet from the circular hydrophobic domains and to form a perforated wetting layer. Here, the contact line is pinned to the boundary between the hydrophobic domains and the surrounding hydrophilic matrix. The contour of the liquid–vapor interface close to the contact line can be described by nodoids, a member of the family of Delaunay surfaces [20, 21], see also Sect. 2.3. Numerical minimizations and the analytic model show that the Laplace pressure of a "thin" perforated wetting film is a monotonously growing function of the liquid volume V per unit cell. The Laplace pressure reaches a maximum value at a volume $V^{\max}$ and decreases as the liquid volume is further increased. Finally, at a critical volume $V^* > V^{\max}$, the "thick" perforated film becomes unstable and forms a homogeneous wetting layer.

3.3. Striped Surface Domains

A wettability pattern of periodic and parallel stripes represents, in addition to circular domains, the second fundamental geometry which has been the subject of several experimental and theoretical studies [3–5]. Linear wettability domains may provide the means to guide liquid in open microfluidic systems or to control the droplet growth during condensation of liquid on the surface. Complete spreading of the wetting liquid on surface patterns is important in printing techniques, which are based on the transfer of ink from the highly wettable domains onto another surface. Printing techniques with a resolution on the micrometer scale would open, e.g., the possibility to print electrical circuits directly onto plane substrates [4]. In any of those applications, the wetting behavior on linear domains like highly wettable stripes will be essential.

We begin our considerations with liquid morphologies on a single wettable stripe and will extend the discussion to related wetting geometry of annular domains as well as to liquid morphologies wetting two or more hydrophilic stripes.

3.3.1. Perfectly Wettable Stripe

Hydrophilic stripes with a material contact angle θ_- close to 0° have been realized by Gau et al. in a hydrophobic silicone rubber (PDMS) matrix where pure water has a contact angle θ_+ of about 110° [3], see the optical micrograph in Fig. 7. As hydrophilic material, MgF_2 has been deposited from the vapor phase through electron microscopy grids forming a layer of less than 20 nm thickness. When cooling the substrate below the dew

point, water condenses onto the hydrophilic MgF_2 pattern of parallel stripes. Each stripe with a length l of several millimeters has a width w = 30 μm and is separated by a hydrophobic stripe of the same width. Since water perfectly wets MgF_2 surfaces, the condensing water spreads along the whole stripe. If the length of the stripe is finite, the liquid forms a cylindrical filament, which grows in size as more liquid condenses. At a certain degree of filling, the liquid–vapor interface of such a homogeneous liquid filament suddenly becomes unstable and decays into a bulge-like droplet, which extends in the form of flat filaments wetting the remaining part of the stripe.

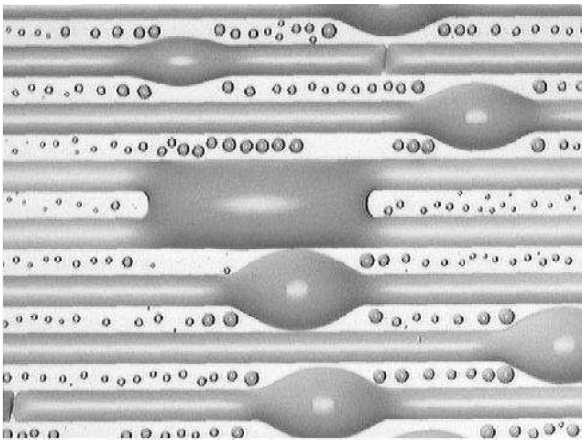

Fig. 7. Optical micrograph showing water morphologies that have been condensed on hydrophilic MgF_2 stripes on a hydrophobic PDMS substrate. The cylindrical homogeneous water filaments have become unstable and form one large bulge-like droplet per filament. In the center, two such bulge-like droplets have merged to a liquid bridge combining two initially separated stripes (image taken from Herminghaus et al. [16])

As pointed out by Gau et al. in [3], the interfacial instability of asymptotically long liquid filaments occurs when the Laplace pressure reaches its maximum value, i.e., when the contact angle θ of the cylindrical filament attains the value 90°. Here, θ denotes the lateral contact angle in a homogeneous part of the filament. "Overfilled" liquid filaments with a contact angle of $\theta > 90°$ may become unstable with respect to a longitudinal exchange of volume since the Laplace pressure is a monotonously decreasing function of the volume in this case. Hence, the liquid in such an overfilled homogeneous filament cannot be in a stable equilibrium. Any small deformation is amplified if the wavelength of the perturbation is

sufficiently large, as it is the case in the Rayleigh-Plateau instability of a free standing liquid cylinder [67]. Corrugations of the liquid–vapor interface with a short wavelength are linked to an area increase and are therefore energetically costly. Hence, the instability is effectively suppressed if the wavelength λ of a shape perturbation is smaller than a threshold wavelength

$$\lambda_c = \frac{w\theta}{\sin\theta}\sqrt{\frac{\pi^2}{\theta^2 - \pi^2/4}}, \tag{4}$$

which is a function of the lateral contact angle θ and stripe width w, see Gau et al. [3]. According to Eq. (4), one can "overfill" liquid filaments up to a lateral contact angle θ larger than 90° on short stripes with a length $l < \lambda_c(\theta)$. For "flat" cylindrical filaments with $\theta < 90°$, however, the Laplace pressure is a monotonously increasing function of the volume. Hence, flat filaments of *arbitrary* length are stable with respect to a longitudinal exchange of volume.

3.3.2. Partially Wettable Stripe

In contrast to perfectly wettable domains, one may expect that a hydrophilic stripe will not be fully covered by liquid if the material contact θ_- angle is finite. Partial wettability implies that sufficiently small liquid droplets are fully located inside the hydrophilic domain. Here, the droplets assume the shape of a spherical cap with the material contact angle θ_-, see Fig. 8a, resp., d. As the liquid volume of the droplet increases, the radius of the contact line grows until it eventually touches the boundary of the hydrophilic stripe and becomes partially pinned. The evolution of the liquid shape during a further increase of volume depends strongly on the material contact angle θ_- on the hydrophilic stripe: For small contact angles θ_-, the droplet grows into an elongated liquid filament, as depicted in Fig. 8b, resp., e. The liquid–vapor interface of a long filament is cylindrical and exhibits noticeable deviations from this ideal shape only close to its ends, only. In addition to the contact angle θ_- on the stripe, these homogeneous filaments are characterized by the lateral contact angle θ at the pinned contact line. If the material contact angle θ_- on the stripe is large, however, the shape of the liquid–vapor interface evolves into a three-dimensional bulge, cf. Fig. 8c, resp., f. In the asymptotic limit of very large volumes $V \gg w^3$, the bulge shape approaches a spherical cap with the

contact angle θ_+ on the hydrophobic matrix. Again, w denotes the width of the stripe.

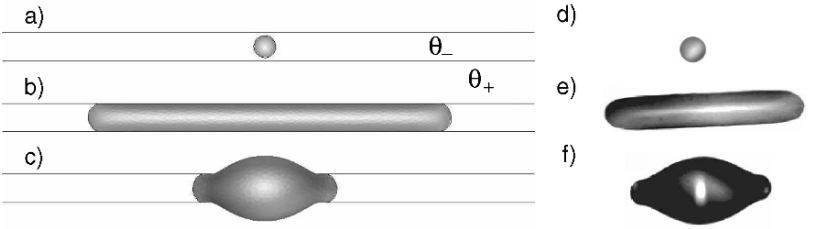

Fig. 8. The three principle droplet morphologies on a single, hydrophilic stripe with a variable contact angle θ_-. (**a**) Small spherical droplet with a circular contact line at a contact angle of $\theta_- = 35°$ and volume $V = 0.05\,w^3$. (**b**) Elongated liquid filament at a contact angle $\theta_- = 35°$ and volume $V = 3\,w^3$. (**c**) bulge morphology at $\theta_- = 45°$ and $V = 10\,w^3$. The contact angle on the hydrophobic substrate is $\theta_+ = 180°$ in all cases. Micrographs in (**d–f**) show corresponding droplet morphologies that have been observed in experiments on hydrophobic substrates decorated with hydrophilic stripes of different wettability (taken from Darhuber et al. [4])

The above scenario describes, for instance, the condensation of liquid on stripes of fixed wettability. Alternatively, one may consider elongated liquid filaments with a fixed volume and vary the contact angle θ_- on the hydrophilic stripes. The liquid forms elongated filaments for small contact angles θ_-, which shrink in length as the contact angle on the stripe is increased. At the same time, the lateral contact angle θ being always larger than θ_- increases until it reaches 90° at a contact angle $\theta_- = \theta_-^*$ on the stripe. In complete analogy to the filaments on perfectly wettable stripes, we find a discontinuous transition to a bulge at $\theta_- = \theta_-^*$. The contact angle θ_-^* where the filament decays into a bulge depends on the liquid volume for short liquid filaments but is virtually independent on the liquid volume for $V \gg w^3$. An analytical model shows, in full agreement with the results of numerical minimizations, that the limit of stability for long liquid filaments becomes

$$\theta_-^* = \arccos\left(\frac{\pi}{4}\right) \approx 38.24^\circ\,, \tag{5}$$

for large volumes, $V \gg w^3$ [5]. Note that expression (5) is only valid for hydrophobic contact angles $\theta_+ > 90°$ on the substrate.

The bulge-like morphology is stable for large volumes and large hydrophilic contact angles but decays into the filament morphology at a certain volume $V = \tilde{V}$ and a contact angle $\theta_- = \tilde{\theta}_-$ which, in general differs from θ_-^*. This transition from a bulge to a filament can be understood from the Laplace pressure in the bulge. At a certain volume, the Laplace pressure in the bulge is high enough to extrude a liquid filament from the main body of the bulge onto the stripe. This process continues until the bulge has completely transformed into a filament since the Laplace pressure of a bulge increases for a decreasing volume while the pressure inside the filament is virtually independent on the filament length.

In contrast to the instability of liquid filaments, the angle $\tilde{\theta}_-$ corresponding to the instability of bulges does not become independent in the limit of large volumes. The points of instability of filaments and bulges can be mapped into the morphology diagram shown in Fig. 9, which displays regions of θ_- and V where the filament F and the bulge B are found as locally or even globally stable morphologies. Filaments F become unstable on the horizontal dashed line in Fig. 9 according to the value given in expression (5). Note that the corresponding lines of instability $(\tilde{V}, \tilde{\theta}_-)$ and (V^*, θ_-^*), and the transition line, where the interfacial energy of both morphologies are equal, merge into a single point at small volume. The existence of such a bifurcation point of equilibrium configurations is not surprising as the liquid morphologies on the hydrophilic stripe need to become sufficiently large to allow a clear distinction between a bulge and a filament. The morphological transition between both morphologies has been experimentally demonstrated by Klinger et al. [17] by use of the electrowetting effect on a stripe electrode, see Fig. 10.

The analytical model describing the filament instability can be extended to "hydrophobic" contact angles $\theta_+ < 90°$. Again, we consider long liquid filaments of fixed volume and vary the wettability on the stripe. While increasing the contact angle θ_- on the stripe, the lateral contact angle θ of the filament at the pinned contact line increases. If, now, the contact angle θ_+ on the substrate is smaller than $90°$, the contact line depins from the boundary of the stripe prior to the above-explained instability for $\theta_+ > 90°$. A cylindrical liquid filament with an unpinned contact lines is

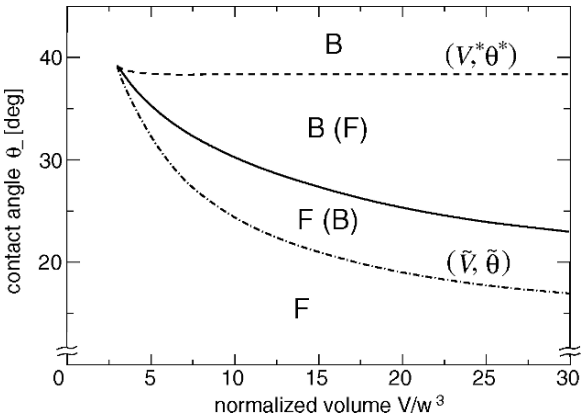

Fig. 9. Morphology diagram for liquid wetting a single hydrophilic stripe of finite contact angle θ_-. A contact angle $\theta_+ = 180°$ is assumed on the hydrophobic matrix. The liquid volume V is given in units of the stripe width, w^3. *Dashed lines* represent stability boundaries of a particular droplet morphology. Liquid filaments F are stable up to the almost horizontal line (V^*,θ_-^*), while the localized bulge morphology B decays into filaments for small volumes $\tilde{V}$ on the lower *dashed dotted line* $(\tilde{V},\tilde{\theta})$. Brackets denote that the corresponding morphology is metastable in this region. The solid line displays the points of transition between both droplet morphologies, i.e., where the interfacial energies are identical

unstable and decays into a bulge [66, 68]. As a consequence, the threshold angle θ_-^* limiting the range of locally stable filament becomes a function of the contact angle θ_+. According to Brinkmann and Lipowsky [5], the analytical model yields a relation

$$\theta_-^* = \arccos\left(\frac{\theta_+}{2\sin\theta_+} - \frac{\cos\theta_+}{2}\right). \tag{6}$$

The stability limit θ_-^* given by expression (5) is asymptotically valid for long filaments, i.e., for large volumes $V \gg w^3$.

3.3.3. Hydrophilic Rings

In the limit of large radii, $R \gg w$, annular domains can be considered as a special case of hydrophilic stripes. Accordingly, liquid morphologies on these "thin" annular domains should be comparable to the morphologies wetting hydrophilic stripes. The spectrum of liquid morphologies on such a

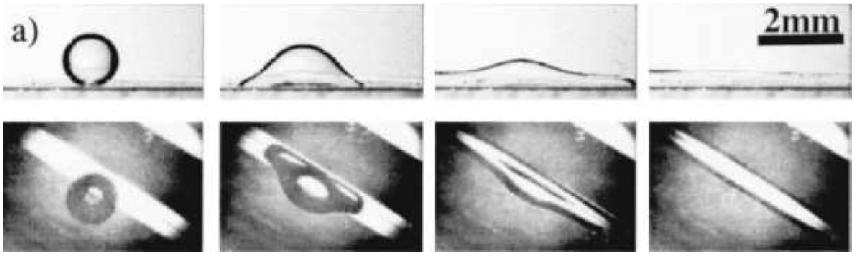

Fig. 10. Optical micrographs of electrowetting-induced transition between an elongated liquid filament and a droplet on a stripe electrode. *Top:* side view, *bottom:* top view. The evaporated stripe is visible as bright area in the top view. The electrode contacting the droplet consists of a thin gold wire aligned parallel to the stripe (images taken from Klingner and Mugele [17])

hydrophilic ring was theoretically and experimentally described by Lenz et al. [21] using solder as a wetting liquid. The molten solder was brought into contact with annular domains of highly wettable copper. As expected by the analogy to the stripe, axially symmetric morphologies that resemble an annular, closed liquid filament are found at small liquid volumes, cf. Fig. 11a. The shape of the liquid–vapor interface of this symmetric configuration can be explicitly parameterized by suitable segments of nodoids, a member of the family of Delaunay surfaces [21]. A second equilibrium morphology being analogous to the bulge morphology on the hydrophilic stripe occurs at larger liquid volume, breaking the exact symmetry of the annular domain. Numerical minimizations of the interfacial energy in the annular geometry are shown in Fig. 11b, c.

In a recent work, equilibrium wetting morphologies on ring-shaped hydrophilic domains were studied by Porcheron et al. [22] minimizing a density functional on a lattice including long-ranged interactions. They found a large spectrum of different morphologies, either partially or fully wetting the hydrophilic annular domain, similar to the morphologies found on hydrophilic stripes. At large volumes, the liquid forms a spherical cap that fully covers the hydrophobic part of the substrate enclosed by the hydrophilic ring, see also the shape minimizations shown in Fig. 11d. Bulges whose contact line has detached from the inner and outer boundary occur in the limit of very narrow annuli [22].

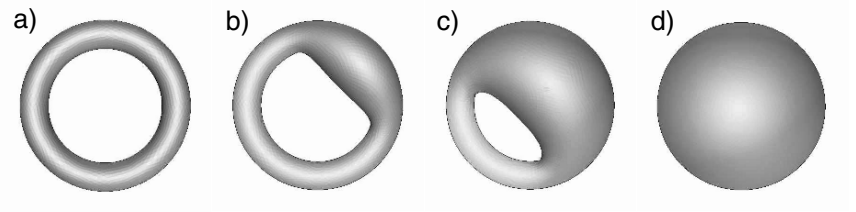

Fig. 11. A series of liquid shapes wetting an annular hydrophilic domain for different volumes, calculated with the software surface evolver. The contact angle on the annular domain is $\theta_- = 0°$, which ensures that the hydrophilic ring is always completely covered by liquid. A contact angle of $\theta_+ = 105°$ was assumed on the hydrophobic part of the substrate. The volume is (**a**) $V = 5.5w^3$ (**b**) $V = 7w^3$ (**c**) $V = 17w^3$, and (**d**) $V = 25w^3$

3.3.4. Liquid Wetting Several Stripes

The morphology of liquid in contact to more than one hydrophilic stripe of width w and separation r is controlled by the normalized distance r/w in addition to the material contact angles θ_- and θ_+, as well as the normalized liquid volume V/w^3.

In the limit of small separations $r \ll w$ between two hydrophilic stripes, one may regard the two stripes and the enclosed hydrophilic part of the substrate as a single hydrophilic stripe with a reduced effective wettability [5]. Hence, it is not surprising that the droplet morphologies found on two stripes resemble those on a single hydrophilic stripe. At small separation $r \ll w$ and large liquid volume $V \gg w^3$, two types of bridges exist in complete analogy with the droplet configurations on a single hydrophilic stripe: Homogeneous filament bridges with an almost cylindrical liquid-vapor interface as shown in Fig. 12a and bulge-like bridges, cf. Fig. 12b, c. The two types of bulge-like bridges are distinguished by the position of their contact line. The morphology in Fig. 12b exhibits a contact line being pinned at the outer domain boundaries of the pair of stripes; for Fig. 12c, it detaches from the domain boundary and makes an excursion across the hydrophobic matrix. Bulge-like bridges are localized along the stripes, whereas filament-like bridges are rather extended and try to maximize the contact with the hydrophilic stripes. Bulge-like bridges exhibit a lower Laplace pressure compared to the filament-like bridges if we compare both morphologies for the same liquid volume, contact angles, and stripe

separation. In the range of large volumes $V \gg w^3$, both types of liquid bridges are symmetric with respect to the symmetry of the hydrophilic stripes.

A distinction between filament-like and bulge-like bridges cannot be made in the range of small liquid volumes. Here, the contact line of the bridging droplet is not necessarily simultaneously pinned to both outer boundaries of the hydrophilic stripes. In this range of volumes, the liquid prefers to form asymmetric shapes because it tries to avoid contact to the hydrophobic stripe enclosed by the two hydrophilic stripes.

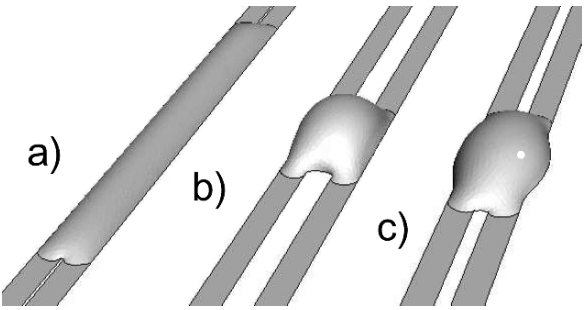

Fig. 12. Liquid morphologies wetting two hydrophilic stripes in the regime of large volumes. (**a**) The liquid forms elongated filament-like bridges on two highly wettable stripes at small separation between the stripes. Localized bulge-like droplets (**b**) and (**c**) appear on less hydrophilic stripes for lower wettabilities or for increased separation

Due to large the spectrum of possible equilibrium shapes for a given volume, the final equilibrium morphology of a liquid droplet placed onto a pattern of parallel hydrophilic stripes depends on its history and the dynamics of the wetting process. This issue was addressed theoretically and experimentally by Léopoldès et al. [69]. They studied the spreading of liquid droplets jetted onto a substrate of parallel hydrophilic stripes. Lattice Boltzmann simulation techniques were used to solve the Navier-Stokes equation governing the dynamics of droplet impact and subsequent spreading of the liquid on the substrate. It turned out that the droplet volume relative to the width of a hydrophilic stripe is the most relevant parameter with respect to the final liquid morphology. The droplet shapes are sensitive to the point of impact and the droplet velocity whenever the ratio of the initial droplet radius to the stripe width is around unity. The final droplet morphologies are identical to the equilibrium morphologies proposed by Brinkmann and Lipowsky [5] and by Darhuber et al. [4].

A periodic modulation of the wettability imposes a strong variation to the contact line curvature of the wetting droplet. This effect shown in the numerical minimization in Fig. 12b can be employed to measure the line tension of the three-phase contact line [70]. The line tension can be introduced as an excess of interfacial energies due to the presence of the three-phase contact line [26]. On chemically homogeneous substrates, this line energy is simple proportional to the length of the contact line. Contrary to interfacial tension, the line tension of the three-phase contact line can assume either negative or positive values [72, 73]. If the contact line is strongly curved, the equilibrium contact angle of the wetting liquid deviates from the equilibrium contact angle of a straight contact line given by the equation of Young-Dupré (3), see Swain and Lipowsky [71].

An experimental study of the systematic variations of the contact angle were performed by Pompe et al. [70]. A large droplet of the wetting liquid is placed onto a pattern of parallel stripes that have been created by micro contact printing of self assembly monolayer. The width of the stripes and the periodicity of the pattern is on the order of several 100 nm. The variations in the local wettability impose spacial oscillation onto the position of the contact line, both with the periodicity of the underlying stripe pattern. High curvatures lead to a modification of the equilibrium condition of Young-Dupré of the form

$$\cos\theta = \cos\theta_{\mathrm{o}} - \frac{c\,\tau}{\gamma_{\mathrm{lv}}}, \tag{7}$$

where θ_{o} is the contact angle given by the equation of Young-Dupré (3), c is the curvature of the contact line in the substrate plane, and τ the line energy per length of the contact line. AFM measurements of liquid profiles (shown in Fig. 13) allow to compute the local contact angle θ and the local curvature c of the contact line. The ratio of line tension τ to surface tension γ_{lv} determines the slope of $\cos\theta$ plotted against the local curvature c of the contact line. The measured values of the contact line tension τ range from 10^{-11} to $10^{-10}\,\mathrm{Jm}^{-1}$ [28, 70] in accordance with theoretical predictions based on the effective interface model and experimental findings.

In the limit of large volumes, the length scale of the corrugation of the three-phase contact line due to the wettability pattern is small compared to the size of the droplet. In this instance, it is useful to define an apparent contact angle of the overall droplet shape, which averages between the hydrophilic and the hydrophobic contact angle of the stripes and substrate

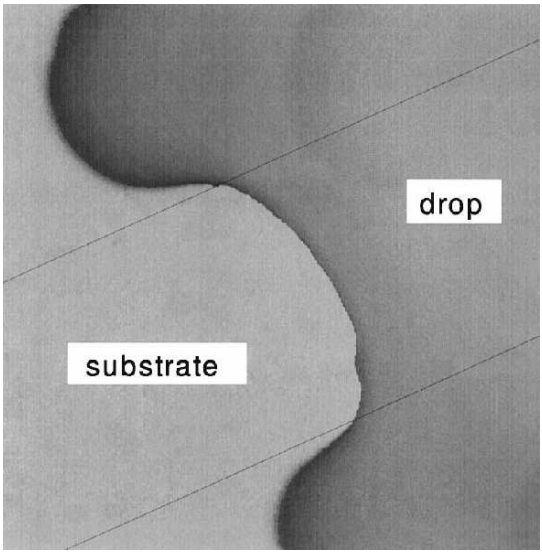

Fig. 13. High resolution AFM micrograph showing the contact line of a hexaethylene glycol droplet on a substrate decorated with a pattern of differently wettable stripes. The corrugation of the contact line is used to determine the dependence of the local contact angle on the curvature c of the contact line. The boundaries of the hydrophilic and hydrophobic stripes are indicated as thin lines (Reprinted with permission from Pompe and Herminghaus [70]. Copyright (2000) by the American Physical Society)

matrix, respectively. Experiments [55, 74] and recent simulations [75] of these droplet morphologies confirm the well-known Cassie equation [76], which expresses the cosine of the apparent contact angle as an average of the cosine of the local material contact angles weighted by the fraction of the wetted area.

4. Wetting of Topographically Patterned Substrates

Liquid wetting morphologies similar to those found on plane substrates with chemical line patterns emerge on chemically homogeneous substrates with linear surface topographies such as steps, wedges, and grooves. Again, pinning of the three-phase contact line is the key to understand the rich variety of liquid equilibrium morphologies. Here, the appearance of different equilibrium morphologies is governed by the specific geometry of the topography, the equilibrium contact angle, and the liquid volume.

In this section, we will again start with an overview of the experimental techniques to prepare surface topographies and continue with the discussion of the liquid morphologies adsorbed to regular arrays of linear surface geometries. Particular attention is paid to the comparison of triangular [23] and rectangular [8] surface grooves, i.e., geometries for potential building blocks in open microfluidic systems.

Variations of the apparent contact angle can be utilized to trigger transitions between different liquid morphologies. Changes in the apparent contact angle allow, for instance, to toggle between dry and completely filled rectangular grooves [9], similar to the electrowetting-induced spreading of liquid on a stripe electrode shown in Fig. 10 [17].

4.1. Substrate Preparation

Depending on $-+$ substrate material, surface grooves can be created by various techniques in a large range of lateral dimensions. We summarize the most common techniques used in fundamental research to fabricate topographically structured substrates: Comparably large grooves down to about 100 μm width can be directly micromachined in metal or polymeric material [12, 13, 77, 78]. Depending on the complexity of the structures, micromachining is a reasonably fast technique to produce single topographic substrates. The surface quality of such fabricated substrates, on the other hand, is often not sufficient for wetting experiments on small length scales.

On submicron length scales topographic structures can be imprinted into molten polymeric material, curable prepolymers, or even glass or silicone from a rigid master [79–86]. The surface quality of such fabricated grooves is good and is basically determined by the surface quality of the master. Similarly, topographic structures of the same length scales can be produced in polymeric materials by soft lithography where silicon rubber molds are used instead of rigid ones [56, 57, 87]. Imprinting techniques are advantageous in case larger quantities of the same kind of substrates are needed, but require more technical effort, e.g. to fabricate a suitable master.

In fundamental research, however, typically only a few substrates with the same topography are needed. Here, it is more important to explore many different surface geometries and wettabilities to map out a larger parameter space. Thus, standard photolithography techniques using glass or silicone substrates with subsequent etching procedures are a good choice. Well-defined small-scaled geometries with triangular and trapezoidal cross section can be fabricated using chemical etching procedures [88]. Anisotropic wet etching of <1, 0, 0>-silicon substrates

with KOH leads to a wedge angle of $\psi = 54.7°$ given by the crystal lattice structure. Another advantage using glass or silicon substrates is that the wettability can be tailored in a wide range by self assembly monolayer as described in Sect. 3.1.

Grooves with rectangular cross section can be fabricated by isotropic reactive ion etching subsequent to the photo lithography. Using this technique, even deep grooves with large aspect ratio can be fabricated.

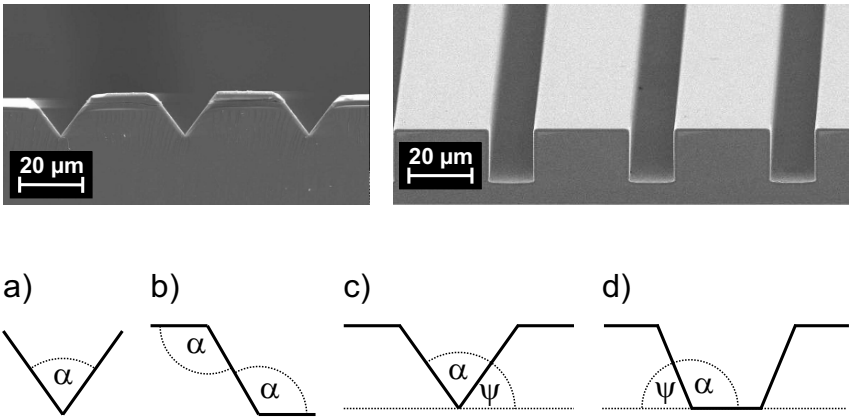

Fig. 14. *Top*: scanning electron micrographs of triangular and rectangular grooves on silicon-wafer fabricated by anisotropic wet etching and isotropic reactive ion etching, respectively. *Bottom*: Sketch of various cross sections (from left to right): infinite wedge (**a**), topographic step (**b**), finite wedge (**c**) and groove geometry (**d**) (top right image courtesy of J.-C. Baret, Philips Research Laboratories, Eindhoven)

Liquid equilibrium morphologies in surface grooves can be created using the same procedures as for chemically patterned substrates: dip coating a sample, dewetting liquid from a sample, or condensing liquid from the vapor phase. To analyze and distinguish the large variety of liquid shapes on topographic substrates, a three-dimensional analysis of the emerging wetting morphologies is usually required. Liquids that can be solidified are highly favorable because they allow to use imaging techniques, which might hardly be possible otherwise. The contour of a groove with small dimensions and the profile of the liquid–vapor interface can, e.g., be characterized by AFM optical or mechanical profiler, or scanning electron microscopy (SEM), as can be seen in Fig. 14.

4.2. Basic Topographies: Infinite Wedge and Step

4.2.1. Infinite Wedge

The most fundamental linear surface topography is an infinite wedge. Because of its invariance with respect to rescaling in all dimensions, a wedge has no intrinsic length scale and is solely characterized by a single angle. This angle can be the opening angle α or, as used in the sequel, the wedge angle $\psi = 90° - \alpha/2$, cf. Fig. 14. Thus, the contact angle θ and the wedge angle ψ are the only control parameters for the appearance of liquid equilibrium morphologies in infinite wedges. In the particular case of Fig. 15, the triangular groove can be regarded as an infinite wedge since the degree of filling is sufficiently small and the liquid wets only the bottom part of the wedge.

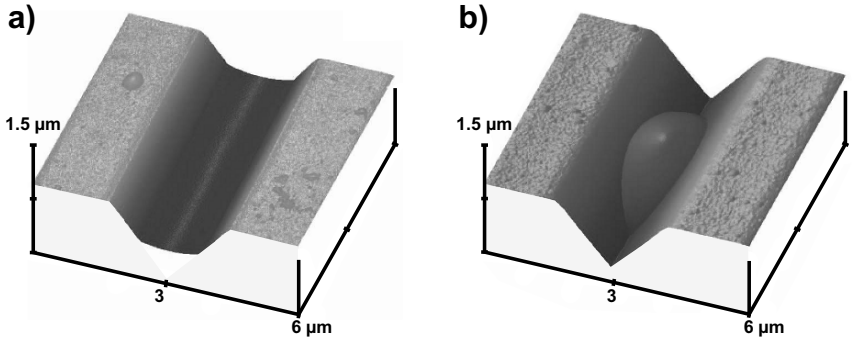

Fig. 15. Atomic force micrographs of polystyrene vapor deposited onto grooved substrates with a wedge angle of $\psi = 54.7°$. (**a**) A liquid wedge with negative mean curvature, $\theta \approx 33°$ and (**b**) droplet wetting morphology with positive mean curvature, $\theta \approx 64°$, cf. [23]

As shown in the AFM micrographs of Fig. 15, there are only two equilibrium wetting morphologies in infinite wedges: spherical droplets with positive mean curvature for $\theta > \psi$ and cylindrical liquid wedges with negative curvature extending along the entire length of the wedge for $\theta < \psi$. Increasing the contact angle θ to the filling angle $\theta = \psi$, the liquid–vapor interface of a liquid wedge becomes marginally stable with respect to a whole spectrum of long wavelength, perturbations. This peculiar behavior can be understood from the scaling invariance of the

liquid configuration in a 2D- cross section of the wedge. Hence, even thermally excited shape fluctuations may become important in a statistical description of the filling transition in infinite wedges [89, 90].

As the contact angle θ approaches the wedge angle ψ from above, the spherical droplets elongate while their tips become more pointed. At the same time, the Laplace pressure tends to zero. Eventually, in the limit $\theta = \psi$, the liquid extends to the entire length of the wedge and the liquid–vapor interface attains a plane configuration.

4.2.2. Tip Shape

It has been first noted by Shuttleworth and Bailey [91] that the tip of a liquid filament in wedges becomes more and more pointed as the contact angle θ approaches the critical filling angle ψ from above, see Fig. 16. They assumed that the liquid–vapor interface at the tip of a filament becomes asymptotically plane. To characterize the geometry of the liquid tip, they introduced the tilt angle β between the liquid–vapor interface and the bottom of the groove. By elementary geometry they derived a relation

$$\cos\beta \cos\psi = \cos\theta , \tag{8}$$

between the contact angle θ, the tilt angle β, and the wedge angle ψ, which holds in the range $\theta > \psi$.

More than 20 years later, Concus and Finn showed that any minimal surface in an infinite wedge, i.e., a surface of zero mean curvature that forms a constant contact angle on the wedge walls, has to be a plane [92]. Since the shape of the wedge bottom is scaling invariant, one can argue that by "zooming in", the tip of a surface of finite constant mean curvature can be asymptotically regarded as a minimal surface on small length scales, i.e., as a surface with zero mean curvature. This implies that the terminal part of the liquid–vapor interface of any equilibrium morphology in the wedge will become asymptotically plane and that, in particular, the predictions of Shuttleworth and Bailey should hold. This is confirmed by experimental measurements of the tilt angle β of the tip by AFM as a function of the contact angle θ, cf. Fig. 16. As a consequence, the transition from filaments to liquid wedges does not happen in an abrupt manner. Instead, one observes a gradual elongation of the droplets involving pointed tips and a final divergence of the total droplet extension while lowering the contact angle θ down to a value below the filling angle $\theta = \psi$ of a wedge.

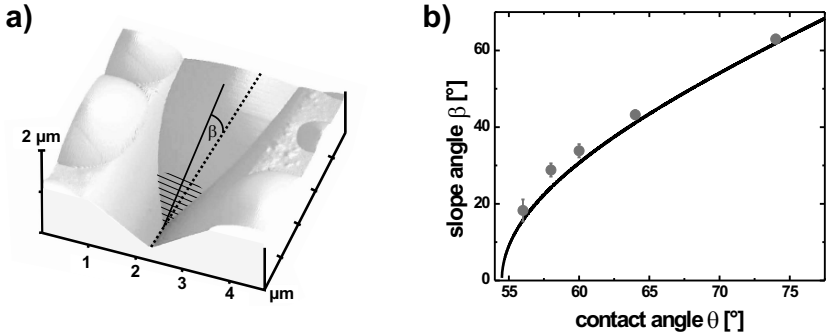

Fig. 16. (**a**) AFM micrograph showing the terminal part of the meniscus of a polystyrene droplet in a triangular groove. The tilt angle β of the terminal meniscus is sketched. (**b**) Tilt angle β for different contact angles θ. Experimental data points were obtained from polystyrene droplets (PS) [23]. The solid line shows the expected relation between β and θ for a wedge angle fixed to $\psi \simeq 54.7^\circ$ according to (8), see also [23]

4.2.3. Topographic Step

Starting from an infinite wedge, one can increase the complexity of the topography by adding corners and edges as sketched in Fig. 14. Consequently, new length scales are introduced in addition to the length scale $\propto V^{1/3}$ given by the volume of the liquid. For a topographic step of height h, one can expect that, besides the step angle α and the contact angle θ, the rescaled volume V/h^3 is a relevant control parameter of liquid morphologies [7]. Provided that either the droplet volume is sufficiently low or the contact angle is smaller than the step angle, the morphologies are identical to those of the infinite wedge. At larger volumes and contact angles larger than the step angle $\theta > \alpha$ the contact line becomes partially pinned to the upper edge of the step. In this regime, elongated liquid structures with an almost homogeneous cross section ("liquid cigar") or localized droplets sitting on the lower semiplane of the sample ("step blobs") can be found, see Fig. 17. A common feature of both morphologies is that a part of the contact line is pinned to the upper edge of the step. For the particular value $\alpha = 90°$, the elongated liquid filament of finite length can be found as a metastable configuration in a range of contact angles $45^\circ < \theta \lesssim 54.5^\circ$, see Brinkmann and Blossey [6].

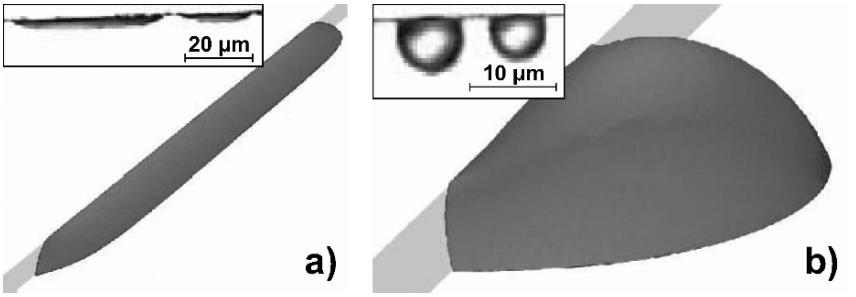

Fig. 17. (**a**) A liquid filament, or liquid "cigar", and a step-blob (**b**) at liquid volumes $V/h^3 = 25$ and step angle $\alpha = 110°$. The contact angle on the substrate is $\theta = 40°$ for the cigar and $\theta = 70°$ for the step-blob. *Insets:* optical micrographs of polystyrene wetting a rectangular step with (**a**) height $h \approx 780\,nm$ and contact angle $\theta \approx 41^\circ$ (**b**) $h \approx 700\,nm$, $\theta \approx 76^\circ$

Going beyond the geometry of an infinite wedge or step, one may consider linear substrate topographies involving more than two kinks. Other simple geometries are symmetric wedges of finite width (three kinks) as we will consider in the following.

4.3. Triangular Grooves

The geometry of a symmetric groove of triangular cross section, sketched in Fig. 14, is determined by a wedge angle ψ and the distance w between the two edges limiting the groove walls to the plane part of the substrate. As mentioned before, the liquid morphologies do not experience the finite extensions of a triangular groove at small liquid volumes $V \ll w^3$ or contact angles $\theta < \psi$. For larger volumes and for contact angles larger than the wedge angle, the finite width of the groove comes into play. The contact line of the wetting liquid may become partially pinned to the edges of the groove, as illustrated in Fig. 18. The spectrum of morphologies consists mainly of localized droplets D, liquid wedges W, and liquid filaments F. Droplets D of small volume are fully confined to the groove (as shown in Fig. 15.b) while larger droplets wet the ridges between two neighboring grooves. The contact line of a liquid filament F is pinned to the edges of the triangular grooves. In contrast to liquid wedges W, filaments extend over a finite length of the groove and exhibit an almost

homogeneous cylindrical liquid–vapor interface with a positive mean curvature. For a fixed wedge angle, the magnitude of the mean curvature of sufficiently long and mechanically equilibrated liquid filaments depends solely on the contact angle and is independent on the liquid volume. Hence, we can approximate the complete shape of a liquid filament by a segment of a cylinder. In this way we obtain a simple analytical model of the liquid configuration, which allows to study the stability of the liquid–vapor interface. A detailed, three-dimensional approximation of the liquid–vapor interface can be reached in numerical minimizations using finite elements, see Sect. 2.3.

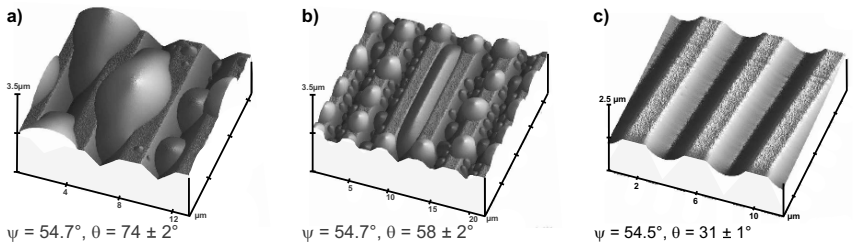

Fig. 18. AFM micrographs of vapor deposited polystyrene structures in grooves with triangular cross section with $\psi \simeq 54.7^{\circ}$. Localized droplets D form at high contact angles θ, while extended filaments F with positive Laplace pressure are found for values of θ close above the wedge angle ψ. Liquid wedges W with a concave meniscus occur for contact angles $\theta < \psi$, cf. [23]

Basically, there are four independent control parameters that govern the appearance of different liquid morphologies in triangular grooves: the liquid volume V, the contact angle θ, the wedge angle ψ, and the width r of the ridges separating two neighboring grooves. It turned out that the contact angle θ and the wedge angle ψ determine the equilibrium shape of the liquid at high volumes $V \gg w^3$.[1] Variations in r influence solely overspilling droplets D in neighboring grooves, which are prone to coalesce and to the formation of larger localized droplet structures. The emergence of filaments F and wedges W, however, is independent on r due to the full confinement of liquid in the grooves. Hence, the appearance of the different

[1]An additional condition $V < w^2 l$ on the volume ensures that the channel of length l and width w is not 'overfilled' by liquid.

droplet morphologies depending on wettability and groove geometry is best illustrated in the form of a morphology diagram in terms of the wedge angle ψ and the contact angle θ. The liquid volume of the droplets as a third control parameter has virtually no influence on the morphologies provided $V \gg w^3$.

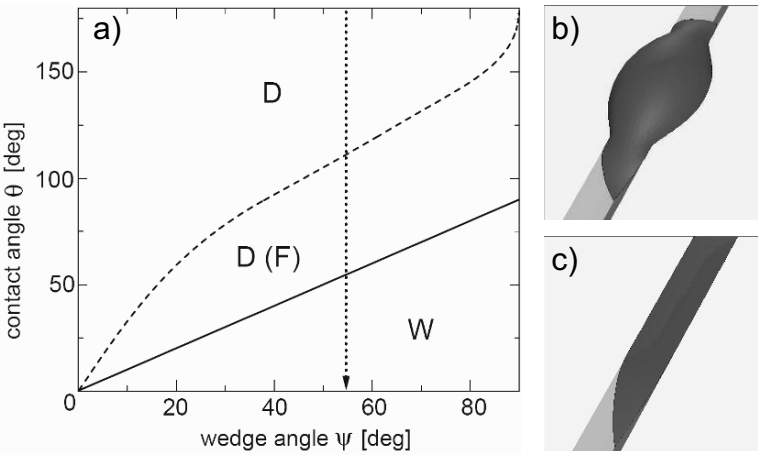

Fig. 19. Morphology diagram of liquid morphologies in triangular grooves in the asymptotic limit of large volumes $V \gg w^3$. The regions where localized droplets and liquid wedges represent the global minimum of the interfacial energy are denoted by D and W, respectively, while (F) indicates the region of metastable elongated filaments, see also [23]. The arrow highlights the special wedge angle $\psi \simeq 54.7^\circ$

A morphology diagram displays regions of relevant control parameters where certain equilibrium droplet shapes exist as locally or globally stable shapes. In the considered regime of large volumes, all liquid filaments F are metastable with respect to droplets D. Metastable configurations are given brackets. The solid line in Fig. 19 separates the regions where droplets D or liquid wedges W are global minima of the interfacial energy. The transition line is simply given by $\theta = \psi$. The dashed line bounds the region of control parameter where filaments F are found as metastable minima to large contact angles.

To illustrate the hysteretic behavior, let us make a gedanken experiment: we start with a lemon-shaped droplet morphology in regime D and decrease the contact angle. The droplet will completely disappear into the

groove forming a liquid wedge W with negative Laplace pressure, if the contact angle is lowered below the solid line in Fig. 19, $\theta < \psi$. But increasing the contact angle back to its original value, the wedge will first undergo a continuous transition to an elongated filament F at $\theta = \psi$ followed by a discontinuous transition to a droplet morphology D when crossing the dashed line in Fig. 19. In regime D(F), liquid filaments and droplets can coexist on a sample, as their appearance depend on the history of the control parameter, liquid, volume or contact angle.

4.4. Rectangular Grooves

In many respects, the equilibrium shapes of liquid droplets found in rectangular grooves are comparable to the morphologies in triangular grooves, but differ in some essential details. The slope of the side walls and a second bottom corner is responsible for the main differences. Rectangular grooves (four kinks) can be regarded as an antisymmetric combination of two topographic steps, both with a step angle $\psi = 90^\circ$. For the wall to wall distance, w, being large compared to the depth of the groove, h, a rectangular groove can be regarded as two independent steps being wetted by two independent morphologies. As the distance w between the opposed topographic steps is decreased such that $w \approx h$ it becomes more and more likely that liquid morphologies with a single meniscus being pinned to both groove edges appear. The combination of liquid structures wetting the entire cross section of the grooves and droplets wetting only a single corner creates a large spectrum of possible equilibrium morphologies in rectangular grooves as we will demonstrate in the following.

It is useful to define a dimensionless aspect ratio $X = w/h$ of the groove depth h to the groove width w to characterize the geometry of a rectangular groove. The most prominent liquid morphologies in rectangular grooves are shown in Fig. 20. Two dominant shapes appear in a wide range of contact angles θ and aspect ratios X: localized, droplet-like shapes D, and elongated liquid filaments F. But in contrast to triangular grooves, the liquid–vapor interface of the liquid filament can be bent either toward the liquid, F–, or toward the vapor phase, F+. The length of a liquid filament depends on the amount of adsorbed liquid while its cross section is independent on the volume, provided that the terminal part of the liquid–vapor interface does not experience the finite length of the groove.

A second class of liquid morphologies appears in combination with the localized droplets and elongated filaments As shown in Fig. 20, the liquid

meniscus of the respective morphology may continue as fine liquid wedges W wetting the corners of the groove to either side of the droplet or filament [8, 23]. The liquid wedges may either be pinned to the upper edges of the groove pW or located in the lower corner of the grooves cW.

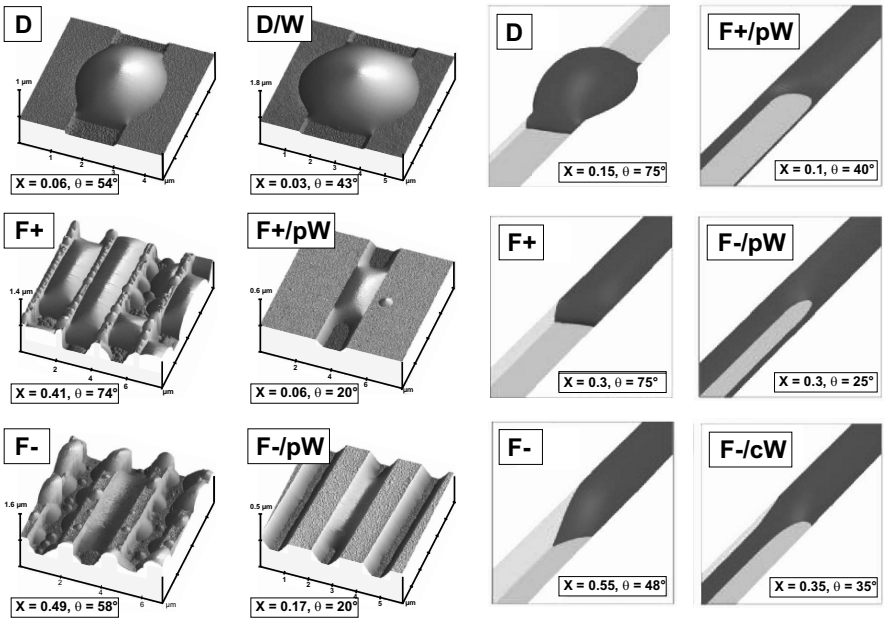

Fig. 20. AFM images (left) and numerically obtained shapes (right) of liquid structures in grooves with rectangular cross section. For contact angles $\theta > 45^\circ$, one observes overspilling droplets D that spread onto the ridges, extended filaments F+ with positive Laplace pressure, and extended filaments F– with negative Laplace pressure. For $\theta < 45^\circ$, one finds droplets D and filaments F that are connected to thin liquid wedges W in the groove corners. The Laplace pressure of filaments and wedges might be positive (+) or negative (–). For details, see [8, 23]

For large liquid volumes, $V \gg w^3$, the liquid shapes are essentially determined by the control parameter contact angle θ and aspect ratio X, similar to the triangular grooves. Here, it is particularly useful to present the various droplets shapes in the morphology diagram shown in Fig. 21 in terms of θ and X as it provides a convenient way to compare the morphologies found in experiments and theory.

All transition lines between different mi were obtained in an analytical model of the liquid morphologies. This model allows to predict the respective regions of contact angles and aspect ratios where globally or locally stable morphologies are found. The morphology diagram Fig. 21 contains the wetting morphologies we identified in Fig. 20: Droplets D, liquid filaments F+ with positive Laplace pressure, and filaments F– with negative Laplace pressure. All these wetting morphologies can coexist with liquid wedges W for contact angles $\theta < 45°$. For small aspect ratios X or large contact angles θ, the liquid forms localized droplet morphologies D. For smaller contact angle or increasing aspect ratio, one may enter the region where filaments with positive Laplace pressure F+ exist as metastable configurations in addition to globally stable droplets D. The boundary of this region is shown as a dashed line in Fig. 21. Decreasing the contact angle even further or increasing the aspect ratio, the Laplace pressure of the filaments lowers and changes its sign when crossing the solid line in the morphology diagram, which denotes filaments of zero mean curvature.

The filament morphology F+ with a positive Laplace pressure is metastable with respect to localized droplets D. Hence, for large liquid volumes, the dashed line represents the largest contact angle for a given aspect ratio for which filaments with positive Laplace pressure can exist as locally stable shapes. Filaments in the regime F– of negative Laplace pressure are always globally stable. Because of the negative Laplace pressure in these filaments, liquid can be spontaneously drawn into rectangular grooves from a large feeding droplet or a liquid reservoir at zero pressure.

Similar to triangular grooves, we find a hysteretic behavior when switching the wettability, e.g., by electrowetting. A large droplet spreads into the grooves in the form of liquid filaments as long as $X > X_o$ with $X_o = (\sqrt{2} - 1)/2 \simeq 0\ 21$ [8] when crossing the solid line between the regimes D(F+) and F–. Liquid wedges will grow out of the filament and coexist with them when lowering the contact angle further below $\theta = 45°$, provided the length of the groove is finite and the liquid volume is large enough. In case the grooves are sufficiently long the wedges will extract the entire liquid from the filament forming just two liquid wedges. The upper three-phase contact line of these liquid wedges will move closer to the upper edge of the groove and as the contact angle is lowered even further. Entering the regime F–/pW, the upper three-phase contact line of the liquid wedge becomes pinned at the edge of the groove. In general, the coexistence of liquid wedges and filaments depends on the length of the grooves and the amount of liquid in the groove.

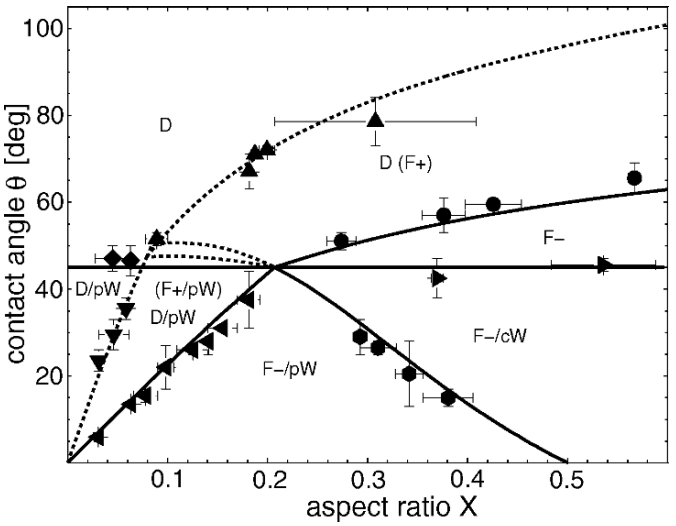

Fig. 21. Morphology diagram of liquid confined to rectangular grooves in the asymptotic limit of large volumes, $V \gg w^3$. The analytical results are in excellent agreement with numerical (not shown) and experimental results (full symbols), cf. Seemann et al. and Khare et al. [8, 23]. The different full symbols denote the respective transition between two regimes. All 185 experimentally determined shapes are fully consistent with the theoretical classification

Most of the morphology transitions are reversible and occur at the same contact angle. But increasing the contact angle above the line indicating filaments of zero mean curvature, the liquid forms metastable filaments with positive Laplace pressure rather than decaying into droplets. These filaments will become unstable when the contact angle enters the regime D above the dashed line. Analogous to the morphologies in triangular grooves, the emergence of liquid morphologies in the regime D(F+) depends on the history of each individual morphology and liquid filaments F+ with positive mean curvature and droplets D may coexist on the same sample.

In sufficiently shallow grooves with $X < X_o$, one may first observe the formation of small pinned liquid wedges growing out of a droplet D while decreasing the contact angle into the regime D/pW. Complete groove filling sets in if we enter the regime F–/pW. Here, the hysteretic behavior during an increase of the contact angle is much more complex and we refer to Seemann et al. [8] for details.

4.5. Switching Equilibrium Morphologies

Liquid filaments advance into triangular and rectangular grooves from droplets or large reservoirs upon decreasing the contact angle. The filling angle is given by the transition line between morphology D (F+) and W in case of triangular grooves, respectively the transition line between D and F– in case of rectangular grooves as shown in the morphology diagrams Figs. 19 and 21.

Hence, combining the topographically structured substrates with a technique, which allows to vary the apparent contact angle, induces morphological transitions which possibly allow for an on-demand imbibition of liquid into grooves, similar to what has been reported for substrates with wettable stripes [17]. But in contrast to planar substrates with wettability patterns, grooves can imbibe liquid even from a reservoir with zero Laplace pressure. Moreover, using grooved substrates may open the possibility to drain liquid completely from grooves by reversibly increasing the wettability. As shown by the morphology diagrams, filling and draining can be done at moderate contact angles. In case of chemically structured substrates, liquid filaments can only be fed by a reservoir with positive Laplace pressure, provided the contact angle of the wettable area is larger that, 0°. But in this regime, up to now, there is no technique available to switch the wettability reversibly. For surface grooves, on the other hand, electrowetting [24] is a versatile and easy-to-use tool to vary the apparent contact angle reversibly in the desired range [9].

The series of optical micrographs in Fig. 22 illustrate typical filling transition experiments varying the wettability by electrowetting on grooves with rectangular cross section [9] and on triangular grooves [23], respectively. The experiment shows a clear threshold behavior for the groove filling, in agreement with the morphology diagrams of Figs. 19 and 21. Because the liquid filaments are always in contact with a large reservoir or droplet, respectively, we do not find a hysteretic behavior. In contrast to the morphology transition of the entire liquid volume, the threshold contact angle for groove filling and draining is identical to the contact angle on the line of zero Laplace pressure.

If the groove filling was solely governed by the relative capillary pressure between the feeding droplet and the filaments, one would expect the filaments to grow indefinitely inside the grooves when the filling threshold is exceeded. However, one readily sees from Fig. 22 that the filaments extend to a finite length, which increases with applied voltage. This finite length is determined by the applied AC-voltage and the finite

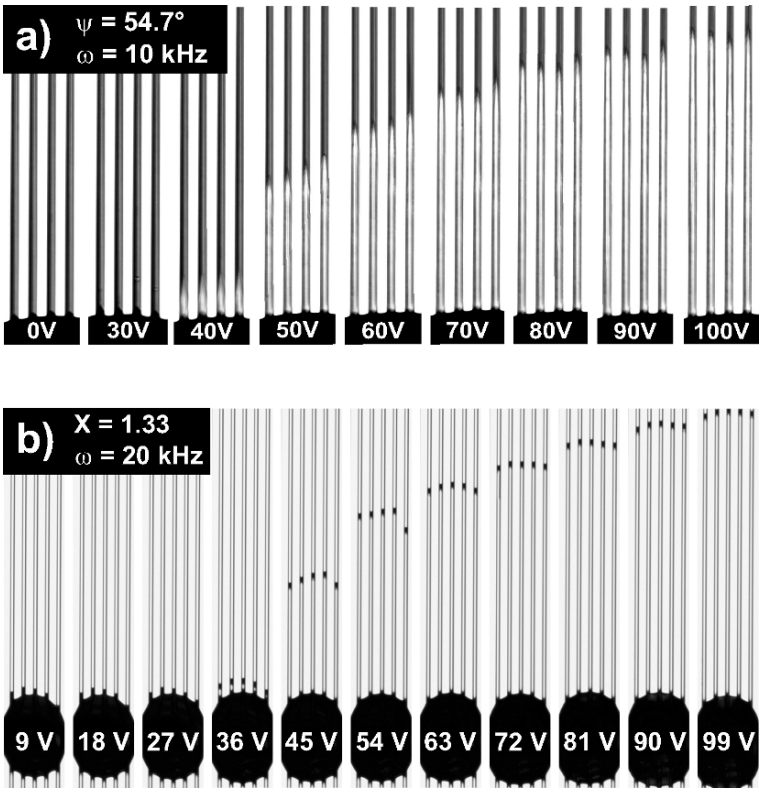

Fig. 22. Top view of a droplet advancing into grooves with (**a**) triangular and (**b**) rectangular cross section for different (equidistant) voltages. The apparent contact angle is lowered using the electrowetting effect applying an AC-voltage between an aqueous solution and a silicone substrate, where ω is the frequency of the applied voltage. Liquid filaments appear bright in the triangular grooves, whereas the tips of a liquid filament appear black in the optical reflection micrographs of rectangular grooves. The length of liquid filaments are in equilibrium at the respective voltage applied [9, 23] (bottom image reprinted with permission from Baret et al. [9]. Copyright (2005) American Chemical Society).

conductivity of the liquid, causing the voltage to drop along the liquid filament [9]. Hence, the apparent contact angle varies along the liquid filament. In equilibrium, the apparent contact angle at the tip of the filament equals the threshold contact angle for the groove filling, as can be determined from the morphology diagrams (Figs. 19 and 21). In case of rectangular grooves, the liquid can be drained reversibly from the grooves

whereas the liquid filaments in triangular grooves decay into isolated droplets via a one-dimensional Rayleigh-Plateau type dewetting process rather than receding back to its feeding droplet [23, 93]. To understand this phenomenon, we recall the idea of Shuttleworth and Bailey [91], as discussed in Sect. 4.2. When approaching the filling angle from above, the tip of the liquid being pulled out of the feeding reservoir becomes more and more pointed while the slope angle of the liquid–vapor interface close to the tip decreases. A close inspection reveals the reason for the instability in triangular grooves during retraction: the contact line of the liquid protruding into the groove is not pinned at the upper edges of the grooves. Hence, during a sudden increase of the apparent contact angle, we generate a liquid filament with positive mean curvature whose contact lines are not pinned. These filaments are dynamically unstable and do not retract into the feeding droplet but decay into a regularly spaced train of isolated droplets.

5. Summary and Outlook

In a wide range of length scales, interfacial energies determine the equilibrium morphologies of nonvolatile liquids wetting substrates decorated with patterns of differently wettable domains. Provided the wettability on these surface domains is sufficiently high, it will be possible to confine the wetting liquid to various shapes if the volume falls into an appropriate range. Here, pinning of the three-phase contact line plays a central role for the mechanical stability of the liquid–vapor interface of the wetting liquid. At large volumes, the liquid–vapor interface of the wetting phase may undergo transitions to configurations characterized by a heterogeneous distribution of liquid on the wettable parts of the surface, as we have illustrated in various examples. These interfacial tension-driven instabilities could pose a serious problem in small scale printing techniques where an even distribution of liquid on the motives is highly desirable. Using the electrowetting effect to tune the wettability, it has been demonstrated for the particular geometry of a wettable stripe that the shape of a liquid droplet can be switched between an elongated and an almost spherical shape. An application of this morphological transition in microfluidics seems to be difficult because the contact angle of the transition to the elongated filament occurs is fairly small for large liquid volumes. The electrowetting effect, on the other hand, is restricted to larger contact angles by saturation effect and contact line instabilities.

Using surface topographies instead of chemically patterned, plane substrates offers a major advantage: The Laplace pressure of liquid morphologies in linear surface grooves of triangular and rectangular cross section can assume negative values in mechanical equilibrium. The sign of the pressure depends, besides on the groove geometry, on the wettability of the surface. An active control of the wettability opens the possibility to draw liquid into the grooves from a reservoir at zero Laplace pressure, e.g., from a large droplet. The contact angle required for imbibition into surface grooves is finite in contrast to plane wetting patterns even for large liquid volumes. This contact angle is determined by the geometry of the groove and becomes large for high aspect ratio grooves. This, in return, allows to adjust the filling angle to the range of contact angles accessible by electrowetting.

Acknowledgment

The authors gratefully acknowledge stimulating discussions with Stephan Herminghaus and Reinhard Lipowsky. Furthermore, we thank Jean-Christophe Baret for fruitful collaboration. Financial support from the MPG and the DFG priority program SPP 1164, grant SE1118 is gratefully acknowledged.

References

1. Lipowsky R (2001) Structured surfaces and morphological wetting transitions. Interface Sci 9:105–115
2. Herminghaus S, Pompe T, Fery A (2000) Scanning force microscopy investigation of liquid structures and its application to fundamental wetting research. J Adhesion Sci Technol 14:1767–1782
3. Gau H, Herminghaus S, Lenz P, Lipowsky R (1999) Liquid morphologies on structured surfaces: From microchannels to microchips. Science 283:46–49
4. Darhuber AA, Troian SM, Miller SM, Wagner S (2000) Morphology of liquid microstructures on chemically patterned surfaces. J Appl Phys 87:7768–7775
5. Brinkmann M, Lipowsky R (2002) Wetting morphologies on substrates with striped surface domains. J Appl Phys 92:4296–4306
6. Checco A, Gang O, Ocko BM (2006) Liquid nanostripes. Phys Rev Lett 96:056104
7. Brinkmann M, Blossey R (2004) Blobs, channels and “cigars”: Morphologies of liquids at a step. Eur Phys J E 14:79–89

8. Seemann R, Brinkmann M, Lange FF, Kramer EJ, Lipowsky R (2005) Wetting morphologies at microstructured surfaces. Proc Natl Acad Sci USA 102:1848–1852
9. Baret JC, Decré M , Herminghaus S, Seemann R (2005) Electroactuation of fluid using topographical wetting transitions. Langmuir 21:12218–12221
10. Darhuber AA, Troian SM, Davis JM, Miller SM, Wagner S (2000) Selective dip-coating of chemically micropatterned surfaces. J Appl Phys 88:5119–5126
11. Darhuber AA, Troian SM (2005) Principles of microfluidic actuation by modulation of surface stresses. Annu Rev Fluid Mech 37:425–455
12. Mann JA, Romero L, Rye RR, Yost FG (1995) Flow of simple liquids down narrow-v grooves. Phys Rev E 52:3967–3972
13. Rye RR, Yost FG, Mann JA (1996) Wetting kinetics in surface capillary grooves. Langmuir 12:4625–4627
14. Yost FG, Rye RR, Mann JA (1997) Solder wetting kinetics in narrow V-grooves. Acta mater 45:5337–5345
15. Blossey R, Bosio A (2002) Contact line deposits on cDNA microarrays: A "twin-spot effect." Langmuir 18:2952–2954
16. Herminghaus S, Gau H, Mönch W (1999) Artificial liquid microstructures. Adv Mater 11:1393–1395
17. Klingner A, Mugele F (2004) Electrowetting-induced morphological transitions of fluid microstructures. J Appl Phys 95:2918–2920
18. Lenz P, Lipowsky R (1998) Morphological transitions of wetting layers on structured surfaces. Phys Rev Lett 80:1920–1923
19. Bechinger C, Muffler H, Schäfle C, Sundberg O, Leiderer P (2000) Submicron metal oxide structures by a sol–gel process on patterned substrates. Thin Solid Films 366:135–138
20. Lenz P, Bechinger C, Schäfle C, Leiderer P, Lipowsky R (2001) Perforated wetting layers from periodic patterns of lyophobic surface domains. Langmuir 17:7814–7822
21. Lenz P, Fenzl W, Lipowsky R (2001) Wetting of ring-shaped surface domains. Europhys Lett 53:618–624
22. Porcheron F, Monson PA, Schoen M (2006) Wetting of rings on a nano-patterned surface: A lattice model study. Phys Rev E 73:041603
23. Khare K, Law BM, Herminghaus S, Brinkmann M, Seemann R (2006) Liquid morphologies on linear surface topographies. submitted.
24. Mugele F, Baret JC (2005) Electrowetting: From basics to applications. J Phys Condens Matter 17:R705–R774
25. Hu DL, Chan B, Bush JWM (2003) The hydrodynamics of water strider locomotion. Nature 424:663–666
26. Rowlinson JS, Widom B (1982) Molecular Theory of Capillarity. Clarendon, Oxford
27. Lipowsky R, Lenz P, Swain PS (2000) Wetting and dewetting of structured and imprinted surfaces. Colloids Surf A 161:3–22
28. Seemann R, Jacobs K, Blossey R (2001) Polystyrene nanodroplets. J Phys Condens Matter 13:4915–4923

29. Checco A, Cai YG, Gang O, Ocko BM (2006) High resolution non-contact AFM imaging of liquids condensed onto chemically nanopatterned surfaces. Ultramicroscopy 106:703–708
30. Do Carmo MP (1976) Differential Geometry of Curves and Surfaces. Prentice Hall, New Jersey
31. Brakke KA (1992) The surface evolver. Exp Math 1:141–165; (1996) The surface evolver and the stability of liquid surfaces. Philos Trans R Soc Lond A 354:2143–2157
32. Sagiv J (1980) Organized monolayers by adsorption. I. Formation and structure of oleophobic mixed monolayers on solid surfaces. J Am Chem Soc 102:92–98
33. Peters RD, Yang XM, Kim TK, Sohn BH, Nealey PF (2000) Using self-assembled monolayers exposed to X-rays to control the wetting behavior of thin films of diblock copolymers. Langmuir 16:4625–4631
34. Peters RD, Yang XM, Kim TK, Nealey PF (2000) Wetting behavior of block copolymers on self assembled films of alkylchlorosiloxanes: Effect of grafting density. Langmuir 16:9620–9626
35. Kim TK, Yang XM, Peters RD, Sohn BH, Nealey PF (2000) Chemical modification of self-assembled monolayers by exposure to soft X-rays in air. J Phys Chem B 104:7403–7410
36. Nissen J, Jacobs K, Radler JO (2001) Chemical modification of self-assembled monolayers by exposure to soft X-rays in air. Phys Rev Lett 86:1904–1907
37. Hoeppener S, Maoz R, Sagiv J (2006) Contact electrochemical replication of electrochemically printed monolayer patterns. Adv Matter 18:1286–1290
38. Bard AJ, Denuault G, Lee C, Mandler D, Wipf DO (1990) Scanning electrochemical microscopy – A new technique for the characterization and modification of surfaces. Acc Chem Res 23:357–363
39. Garcia R, Calleja M, Perez-Murano F (1998) Local oxidation of silicon surfaces by dynamic force microscopy: Nanofabrication and water bridge formation. Appl Phys Lett 72:2295–2297
40. Dai HJ, Franklin N, Han J (1998) Exploiting the properties of carbon nanotubes for nanolithography. Appl Phys Lett 73:1508–1510
41. Maoz R, Cohen SR, Sagiv J (1999) Nanoelectrochemical patterning of monolayer surfaces: Toward spatially defined self-assembly of nanostructures. Adv Mater 11:55–61
42. Geissler M, Xia YN (2004) Patterning: Principles and some new developments. Adv Mat 16:1249–1269
43. Gau H, Herminghaus S (2000) Ripening of ordered breath figures. Phys Rev Lett 84:4156–4159
44. Denkov ND, Velev OD, Kralchevsky PA, Ivanov IB, Yoshimura H, Nagayama K (1992) Mechanism of formation of 2-dimensional crystals from latex particles on substrates. Langmuir 8:3183–3190
45. Denkov ND, Velev OD, Kralchevsky PA, Ivanov IB, Yoshimura H, Nagayama K (1993) 2-dimensional crystallization. Nature 361:26–26

46. Burmeister F, Schäfle C, Matthes T, Bohmisch M, Boneberg J, Leiderer P (1997) Colloid monolayers as versatile lithographic masks. Langmuir 13:2983–2987
47. Widawski G, Rawiso M, Francois B (1994) Self-organized honeycomb morphology of star-polymer polystyrene films. Nature 369:387–389
48. Heier J, Kramer EJ, Walheim S, Krausch G (1997) Thin diblock copolymer films on chemically heterogeneous surfaces. Macromolecules 30:6610–6614
49. Wang R, Parikh AN, Beers JD, Shreve AP, Swanson B (1999) Nonequilibrium pattern formation in Langmuir-phase assisted assembly of alkylsiloxane monolayers. J Phys Chem B 103:10149–10157
50. Gleiche M, Chi LF, Fuchs H (2000) Nanoscopic channel lattices with controlled anisotropic wetting. Nature 403:173–175
51. Piner RD, Zhu J, Xu F, Hong SH, Mirkin CA (1999) "Dip-pen" nanolithography. Science 283:661–663
52. Ginger DS, Zhang H, Mirkin CA (2004) The evolution of dip-pen nanolithography. Angew Chem Int Ed 43:30–45
53. Wouters D, Schubert US (2004) Nanolithography and nanochemistry: Probe-related patterning techniques and chemical modification for nanometer-sized devices. Angew Chem Int Ed 43:2480–2495
54. López GP, Biebuyck HA, Frisbie CD, Whitesides GM (1993) Imaging of features on surfaces by condensation figures. Science 260:647–649
55. Drelich J, Miller JD, Kumar A, Whitesides GM (1994) Wetting characteristics of liquid drops at heterogeneous surfaces. Colloids Surf A 93:1–13
56. Xia YN, Whitesides GM (1998) Soft lithography. Annu Rev Mater Sci 28: 153–184
57. Gates BD, Xu QB, Stewart M, Ryan D, Willson CG, Whitesides GM (2005) New approaches to nanofabrication: Molding, printing, and other techniques. Chem Rev 105:1171–1196
58. Kumar A, Whitesides GM (1994) Patterned condensation figures as optional diffraction gratings. Science 263:60–62
59. Herminghaus S, Fery A, Reim D (1997) Imaging of droplets of aqueous solutions by tapping-mode scanning force microscopy. Ultramicroscopy 69:211–217
60. Rehse N, Knoll A, Konrad M, Magerle R, Krausch G (2001) Surface reconstruction of an ordered fluid: An analogy with crystal surfaces. Phys Rev Lett 87:035505
61. Luo CX, Xing RB, Zhang ZX, Fu J, Han YC (2004) Ordered droplet formation by thin polymer film dewetting on a stripe-patterned substrate. J Colloid Interface Sci 269:158–163
62. Kim E, Xia YN, Whitesides GM (1996) Micromolding in capillaries: Applications in materials science. J Am Chem Soc 118:5722–5731
63. Yang PD, Deng T, Zhao DY, Feng PY, Pine D, Chmelka BF, Whitesides GM, Stucky GD (1998) Hierarchically ordered oxides. Science 282:2244–2246
64. Donald AM (2003) The use of environmental scanning electron microscopy for imaging wet and insulating materials. Nat Mater 2:511–516

65. Lipowsky R, Brinkmann M, Dimova R, Franke T, Kierfeld J, Zhang XZ (2005) Droplets, bubbles, and vesicles at chemically structured surfaces. J Phys Condens Matter 17:S537–S558
66. Lenz P, Lipowsky R (2000) Stability of droplets and channels on homogeneous and structured surfaces. Eur Phys J E 1:249–262
67. Lord Rayleigh (1878) On the instability of jets. Proc London Math Soc 10: 4–13
68. Brinkmann M, Kierfeld J, Lipowsky R (2005) Stability of liquid channels or filaments in the presence of line tension. J Phys Condens Matter 17:2349–2364
69. Léopoldés J, Dupuis A, Bucknall DG, Yeomans JM (2003) Jetting micron-scale droplets onto chemically heterogeneous surfaces. Langmuir 19:9818–9822
70. Pompe T, Herminghaus S (2000) Three-phase contact line energetics from nanoscale liquid surface topographies. Phys Rev Lett 85:1930–1933
71. Swain PS, Lipowsky R (1998) Contact angles on heterogeneous surfaces: A new look at Cassie's and Wenzel's laws. Langmuir 14:6772–6780
72. Indekeu JO (1992) Line tension near the wetting transition: Results from an interface displacement model. Physica A 183:439–461
73. Indekeu JO (1994) Line tension at wetting. Int J Mod Phys B 8:309–345
74. Drelich J, Wilbur JL, Miller JD, Whitesides GM (1996) Contact angles for liquid drops at a model heterogeneous surface consisting of alternating and parallel hydrophobic/hydrophilic strips. Langmuir 12:1913–1922
75. Brandon S, Haimovich N, Yeger E, Marmur A (2003) Partial wetting of chemically patterned surfaces: The effect of drop size. J Colloid Interface Sci 263:237–243
76. Cassie ABD (1948) Contact angles. Discuss Faraday Soc 3:11–16
77. Rye RR, Mann JA, Yost FG (1996) The flow of liquids in surface grooves. Langmuir 12:555–565
78. Bruschi L, Carlin A, Mistura G (2002) Complete wetting on a linear wedge. Phys Rev Lett 89:166101
79. Chou SY, Krauss PR, Renstrom PJ (1995) Imprint of sub-25 nm vias and trenches in polymers. Appl Phys Lett 67:3114–3116
80. Chou SY, Krauss PR, Renstrom PJ (1996) Imprint lithography with 25-nanometer resolution. Science 272:85–87
81. Haisma J, Verheijen M, vandenHeuvel K, vandenBerg J (1996) Mold-assisted nanolithography: A process for reliable pattern replication. J Vac Sci Technol B 14:4124–4128
82. Heckele M, Bacher W, Muller KD (1998) Microsyst Technol 4:122–124
83. Bender M, Otto M, Hadam B, Vratzov B, Spangenberg B, Kurz H (2000) Fabrication of Nanostructures using a UV-based imprint technique. Microelectron Eng 53:233–236
84. Colburn M, Grot A, Choi BJ, Amistoso M, Bailey T, Sreenivasan SV, Ekerdt JG, Willson CG (2001) Patterning nonflat substrates with a low pressure, room temperature, imprint lithography process. J Vac Sci Technol B 19:2162–2172

85. Otto M, Bender M, Hadam B, Spangenberg B, Kurz H (2001) Characterization and application of a UV-based imprint technique. Microelectron Eng 57:361–366
86. Chou SY, Keimel C, Gu J (2002) Ultrafast and direct imprint of nanostructures in silicon. Nature 417:835–837
87. Seemann R, Kramer EJ, Lange FF (2004) Patterning of polymers: Precise channel stamping by optimizing wetting properties. New J Phys 6:111
88. Madou MJ (1997) Fundamentals of Microfabrication. CRC Press, Boca Raton, FL
89. Parry AO, Rascon C, Wood AJ (2000) Critical effects at 3D wedge wetting. Phys Rev Lett 85:345–348
90. Rascon C, Parry AO (2000) Geometry-dominated fluid adsorption on sculpted solid substrates. Nature 407:986–989
91. Shuttleworth R, Bailey GLJ (1948) The spreading of a liquid over a rough solid. Discuss Faraday Soc 3:16–22
92. Concus P, Finn R (1969) On behavior of a capillary surface in a wedge. Proc Natl Acad Sci USA 63:292–299
93. Khare K, Law BM, Gurevich E, Brinkmann M, Herminghaus S, Seemann R (2007) Dewetting of liquid filaments in wedge-shaped grooves. submitted